Large Airways

2

Pierluigi Ciet, Mark C. Liszewski, and Edward Y. Lee

Introduction

Large airway magnetic resonance (MR) imaging is a relatively new technique in thoracic imaging, with chest radiography (CXR) and computed tomography (CT) being the most used modalities [1]. However, the lack of ionizing radiation makes MR imaging an attractive alternative to CT particularly in the pediatric population [2]. Disorders of the respiratory system are quite common and of great importance in pediatrics, including both lung and airway disorders [3]. While CXR is most often the first step for imaging disorders of the lungs, CT is the technique with the highest sensitivity to assess airway pathology [4]. The rapid improvement of MR imaging techniques has made it feasible to obtain similar image quality to CT but with the unparalleled advantage of combined structural and functional imaging without radiation exposure [5].

In this chapter, MR imaging techniques for evaluating the large airways and normal anatomy in pediatric patients are discussed. In addition, various congenital and acquired disorders commonly affecting infants and children are reviewed including clinical features, characteristic MR imaging findings, and current treatment approaches.

P. Ciet (✉)
Department of Radiology and Nuclear Medicine, Department of Pediatric Pulmonology, Sophia Children's Hospital Erasmus Medical Center, Rotterdam, South-Holland, The Netherlands
e-mail: p.ciet@erasmusmc.nl

M. C. Liszewski
Division of Pediatric Radiology, Departments of Radiology and Pediatrics, The Children's Hospital at Montefiore and Montefiore Medical Center, Bronx, NY, USA

E. Y. Lee
Division of Thoracic Imaging, Department of Radiology, Boston Children's Hospital, Harvard Medical School, Boston, MA, USA

Magnetic Resonance Imaging Techniques

Patient Preparation

Patient age is an essential factor to consider when preparing patients for large airway MR imaging. In pediatric patients who are unable to follow instructions, including most patients younger than 5 years and patients with cognitive delay, free-breathing MR imaging techniques with or without anesthesia are mandatory [6]. The risks of anesthesia should be discussed with the referring physician and the parents and weighed with the potential benefits of the MR imaging examination. Possible negative sequelae of deep sedation on the developing brain have been shown in animal models [6]. When sedated, the patient needs to be closely monitored, ensuring appropriate heart rate, blood pressure, and oxygenation. A possible alternative to sedation in neonates is the "feed and swaddle" technique [7], where the child is fed immediately before the examination and then placed in the scanner after being swaddled. This technique works well in imaging of stationary body parts such as the brain. However, for chest imaging, its use is frequently limited due to respiratory motion, which is accentuated by the high respiratory rates of neonates.

Cardiac and respiratory rate are two crucial factors that determine image quality in the neonatal patient age group [6]. Even with an optimized MR imaging protocol including sequences with low motion sensitivity, such as those with radial and of helicoidal k-space acquisitions, unexpected patient movement can make a scan non-diagnostic. To reduce respiratory motion, the anesthesiologist can hold respiration at end-inspiration or end-expiration in a controlled setting where patient's vital signs are constantly monitored [6]. Alternatively, a breath-hold state can be recreated through hyperventilation. The radiologist is respon-

E. Y. Lee et al. (eds.), *Pediatric Body MRI*, https://doi.org/10.1007/978-3-030-31989-2_2

sible to keep the scan time as short as possible and at the same time to ensure diagnostic image quality. A short scan time is also important to limit the development of atelectasis, which can obscure underlying abnormalities [8]. After the MR imaging is completed, the patient is usually monitored in a controlled environment until discharge from the radiology department to ensure full recovery from anesthesia.

Older pediatric patients (usually older than 5 years), who can follow directions, may attempt to undergo MR imaging without sedation. Preparation before the MR imaging examination greatly improves the success rate in this pediatric patient group. This preparation consists of familiarizing the patient with the noisy environment of MR scanner and practicing the breathing maneuvers that will be performed during the MR imaging examination [6]. A mock scanner (Fig. 2.1) can be used to reproduce similar noises of real MR imaging sequences and the movement of the table. Moreover, the patient can understand the importance of laying still and rehearse specific maneuvers in the supine position recreating the same conditions as during the MR imaging scan [9]. Coaching and scanning with an MR imaging-compatible spirometer helps standardize lung volume assessment [9]. This device allows real-time monitoring of maximal inspiratory and expiratory volumes that can be used as references to trigger MR imaging acquisition during the scan [9]. Finally, to reduce possible anxiety related to the scan, parents should be allowed to stay in the MR imaging room with the child and distraction methods, such as projecting a movie, can be used to help the children feel comfortable [6].

Fig. 2.1 Mock scanner for pediatric patient training. In the mock scanner, pediatric patients familiarize themselves with the noisy environment of the MR imaging scanner and can rehearse breathing maneuvers

MR Imaging Pulse Sequences and Protocols

Unlike lung imaging, where 1.5 Tesla (T) systems are more suitable to achieve high signal-to-noise ratio (SNR) thanks to lower T2 star ($T2^*$) dephasing and susceptibility artifacts, large airway MR imaging is more suitable at higher magnetic fields, such as 3T or higher [2]. These systems can allow faster performance especially for dynamic imaging (because of higher SNR and slew rate). Another critical factor for better image quality in large airway MR imaging is choosing the correct receiver coil. Close-fitting, high-density, receiver phase-array coils are of key importance [2]. Phase-array coils provide higher SNR by virtue of the closer proximity to the large airways but also allow for shorter acquisition time through the use of parallel imaging [2].

Optimal coil designs differ depending on the patient anatomy; for thoracic MR imaging the coils most frequently used are arrays with 8–32 receiver channels. Infants and young children can benefit from the use of small flexible coils directly in contact with the target area, while older patients can be imaged using a torso or head/neck/spine (HNS) coil. A loose HNS coil design has the advantage of a small anterior coil receiver, which provides a tighter fit when imaging the upper airways compared to a torso coil (Fig. 2.2). This is especially true in older girls with fully developed breasts or muscular boys with prominent pectoral muscles. Further improvements in SNR could be obtained with dedicated cape-like coils

Fig. 2.2 Coil selection and placement for a 7-year-old girl. (**a**) 8-channel head/neck/spine (HNS) phase-array coil (GE), consisting of an anterior portion that is freely adaptable to variable thoracic sizes allowing for closer-fitting than standard torso coils in children. (**b**) 6-channel coil prototype for upper airway imaging built in the Erasmus Medical Center (Rotterdam, The Netherlands) in collaboration with Machnet B.V. and Flick Engineering B.V. (Winterswijk, The Netherlands)

tailored for large airway MR imaging. MR imaging techniques for large airway imaging are summarized in the following sections. A dedicated protocol for large airway MR imaging is presented in Table 2.1.

Static MR Large Airway Imaging

Complete MR airway imaging relies on both end-inspiratory and end-expiratory acquisitions. This can only be achieved in compliant pediatric patients. Breath-hold time needs to be tailored to patient's age; therefore, younger patients require shorter acquisition times in the range of 8–12 seconds. Such scan times are achievable with several two dimensional (2D) and three-dimensional (3D) sequences. In pediatric patients who cannot follow instructions, free-breathing acquisitions combined with respiratory triggering or navigation allow diagnostic image quality, though at the expense of longer acquisition times.

2D Techniques

Fast Spin-Echo Sequences Fast spin-echo (FSE) or turbo spin-echo (TSE) sequences have low sensitivity to magnetic susceptibility artifacts and can achieve sub-second acquisition times (e.g., single-shot FSE scans) [2]. A typical sequence is the 2D T2-weighted single-shot FSE scan, known under different acronyms depending on the MR imaging scan manufacturer [2]. Single-shot FSE techniques have high sensitivity and high SNR for fluid detection. As all T2-weighted sequences, they are suitable to assess bronchial wall thickening and mucus plugging (Fig. 2.3). Bronchial walls can be further highlighted with blood suppression techniques, such as those using a black blood (BB) preparation. BB preparation involves the application of two radio-frequency (RF)-inversion pulses in close succession (non-selective and selective excitation and a corresponding inversion

Table 2.1 MR imaging protocols for large airway imaging

Sequence type	Brand name (Brand)	Weighting	Acquisition setting and duration	Spatial resolution and orientation	Temporal resolution	Scan parameters	MR imaging system
Static airway evaluation							
2D Fast spin echo	PROPELLER (GE) BLADE (Siemens) MultiVane (Philips)	T2-weighted Black blood	End-expiratory with navigator echo triggering 3–7 min according respiratory pace and pattern	FOV = 380–400 mm Matrix = 200 × 200 SL = 5–6 mm Axial and coronal	Low	TR = respiratory rate (2–5 s) TE = short–medium (25–60 ms) FA = 90°/150° ± FAT saturation BW = low–medium	1.5T and 3.0T
2D SSFP	FIESTA (GE) TrueFISP (Siemens) Balanced-FFE (Philips)	T1/T2-weighted Bright blood	12–20 s Breath-hold	FOV = 400 mm Matrix = 160 × 160 SL = 2.5–5 mm Axial and coronal	High	TR = shortest (<4 ms) TE = shortest (<2 ms) FA = 40° BW = high	1.5T
3D Fast spin echo	CUBE (GE) SPACE (Siemens) VISTA (Philips)	T2-weighted Black blood	End-expiratory with pencil-beam navigator triggering 5–7 min	FOV = 320 mm Matrix = 160 × 160 SL = 2 mm Sagittal or coronal	Low	TR = respiratory rate (2–5 s) TE = medium (60 ms~) FA = 90°/variable flip train BW = medium–high Echo train length = 80–140 FAT saturation	1.5T and 3.0T
3D RF spoiled gradient echo	SPGR (GE) VIBE (Siemens) THRIVE (Philips)	PD to T1-weighted	Breath-hold 10–12 s (inspiratory and expiratory)	FOV = 400 mm Matrix = 200 × 200 SL = 2 mm Isotropic voxel, as low as 8 mm^3 Sagittal or coronal	High	TR = shortest (<1.7 ms) TE = shortest (<0.7 ms) FA = 2° BW = medium–high	1.5T and 3.0T
3D RF spoiled gradient echo	StarVIBE (Siemens) Clinically not available for GE or Philips	PD to T1-weighted	Free breathing 3–5 min	FOV = 400 mm Matrix = 320 × 320 SL = 1.2– 4 mm voxel (2–5 mm^3) Axial	Low	TR = 7.46 ms TE = 2.46 ms FA = 9° BW = medium	1.5T and 3.0T
3D Two-point DIXON RF spoiled gradient echo	LAVA Flex (GE)	PD to T1-weighted Water-only, fat-only, in-phase, and out-of-phase contrast	Breath-hold (10 s) Free breathing (pencil-beam navigator)	FOV = 260 mm Matrix = 128 × 128 SL = 3 mm Voxel (<3 mm^3) Axial	High	TR = 3.7–4.5 ms TE = min full (<2.0 ms) FA = 2°–10° BW = medium–high	1.5T and 3.0T
3D Ultra-short TE gradient echo	UTE (GE) SPIRALVIBE (Siemens) MultiVane (Philips)	PD-weighted Slight T1-weighting depending on readout flip angle chosen UTE	7–10 min Free breathing	FOV = 360 mm Voxel size = 1–8 mm^3 Sagittal or coronal	Low	TR = short (<5 ms) TE = 0.07 ms BW = medium–high	1.5T and 3.0T
3D Ultra-short TE gradient echo	VNAV (GE) SPIRALVIBE (Siemens)	PD-weighted Slight T1-weighting depending on readout flip angle chosen Silent	7–10 min Free breathing	FOV = 360 mm Matrix = 360 × 360 × 360 Sagittal or coronal	Low	TR = shortest (<1.3 ms) TE = 0 ms BW = medium–high	1.5T and 3.0T

Sequence type	Brand name (Brand)	Weighting	Acquisition setting and duration	Spatial resolution and orientation	Temporal resolution	Scan parameters	MR imaging system
Dynamic airway evaluation							
2D Steady-state free precession gradient echo – SSFP	FIESTA (GE) TrueFISP (Siemens) Balanced-FFE (Philips)	T1/T2-weighted Inflow enhancement	3–4 minutes hyperventilation Coverage larynx to carina ~ 4 s per slice position	FOV = 450 × 160 mm Matrix = 128 × 128 SL = 8 mm Axial	4–5 images/s	TR = shortest (1.8 ms–2.4 ms) TE = shortest (<1.2 ms) FA = 35° BW = medium–high	1.5T
3D RF spoiled gradient echo	TRICKS (GE) TWIST (Siemens) 4D-TRAK (Philips)	PD to T1-weighted	20 s Forced expiration, free breathing, or hyperventilation	FOV = 300 mm Matrix = 80 × 100 SL = 3.2 mm Sagittal	<400 ms/ volume	TR = shortest (<2 ms) TE = minimum (<1.1 ms) FA = 2° BW = medium–high	1.5T and 3.0T

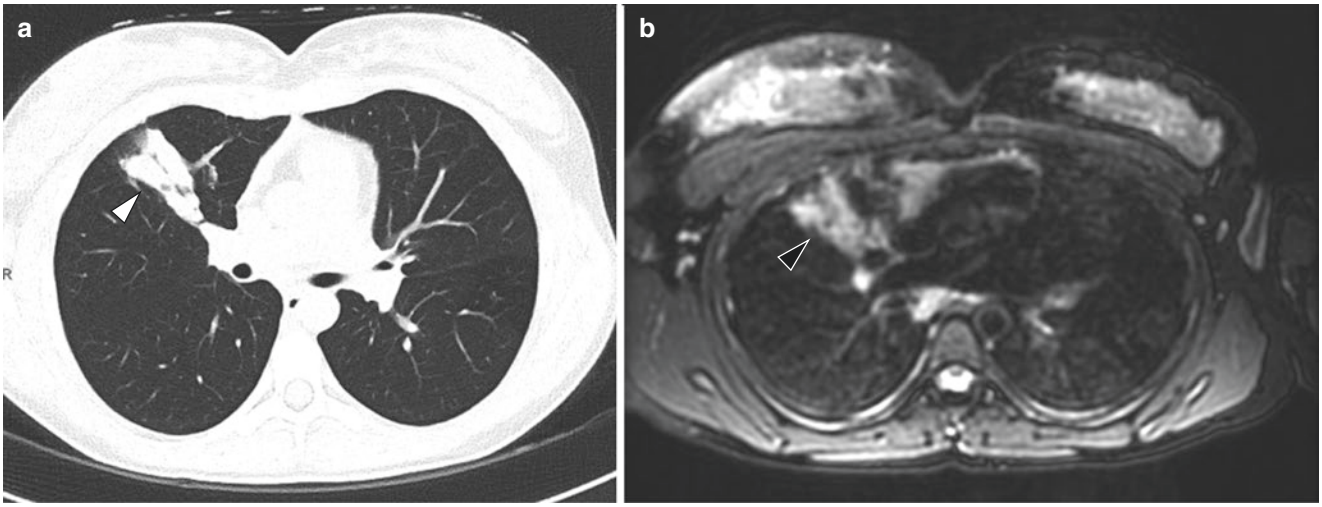

Fig. 2.3 Cystic fibrosis and allergic bronchopulmonary aspergillosis in a 16-year-old girl. (**a**) Axial nonenhanced lung window setting CT image obtained at end-expiration shows impacted mucus and bronchiectasis (*white arrowhead*) in the right middle lobe. (**b**) Axial nonenhanced isotropic three-dimensional (3D) CUBE (GE) T2-weighted MR image obtained at end-expiration shows impacted mucus and bronchiectasis (*black arrowhead*) in the right middle lobe

time TI) in order to cancel all signal deriving from the blood. These sequences have a very high specific absorption ratio (SAR). Especially with small children, single-shot FSE requires longer wait time between slices to stay within safety norms and avoid patient heating.

Fast Spin Echo with Helical K-Space Acquisition PROPELLER (Periodically Rotated Overlapping ParallEL Lines with Enhanced Reconstruction) is a particular FSE non-breath-hold readout that collects imaging data using rotating k-space bands or blades, which is more resistant to respiratory and cardiac motion artifact [2]. The collection of blades oversamples the center of k-space, thus producing better SNR and reducing rotational and translational in-plane motion occurring between k-space segments collected on each blade [2]. This sequence is suitable for non-cooperative pediatric patients and can be combined with prospective respiratory-gated techniques (i.e., using pen-beam navigators or pneumobelts), to further reduce the effects of motion. Full axial chest coverage (approximately 25–30 cm craniocaudally) can be achieved in 4–7 minutes with good spatial resolution (1 × 1 × 5 mm) [2]. To enhance detection of bronchial wall thickening, bronchiectasis, and bronchial wall lesions, long TE settings are preferred in order to reduce signal from vascular structure and to increase water detection (Fig. 2.4).

Steady-State Free Precession Technique Steady-state free precession (SSFP) techniques are a group of gradient-recalled echo (GRE) sequences, which generate T2/T1 weighting with medium to high readout flip angle (FA) settings (>30°) using very short repetition times (TR). On these sequences tissues with water-like characteristics are hyperintense, such as mucus plugs in the airways [2]. 2D SSFP scans allow fast acquisitions of the entire thorax in a single breath-hold with good SNR. Moreover vascular structures also appear bright on SSFP (bright blood), allowing assessment of mediastinal vessels for possible compression of large airways. A limitation of this sequence is its sensitivity to magnetic field inhomogeneities, which can become problematic at higher magnetic field strengths (i.e., 3T). SSFP also has an intensive SAR profile (though much less than single-shot FSE), which with high flip angles and at higher field strengths can exceed the maximal safety level allowed in MR imaging.

3D Techniques

Gradient Recalled Echo Sequences Short and ultra-short echo time GRE sequences are typically considered as the most robust sequence for chest MR imaging [2]. These sequences when used with short or ultra-short echo times can minimize the signal loss created by air-tissue interfaces thus providing high SNR. GRE are usually collected with minimum TR and TE settings to achieve the best SNR possible and the shortest acquisition time. For isotropic voxel sizes between 2 and 3.5 mm, a capable MR imaging system can provide a TE ranging from 0.4 to 0.7 ms with an acquisition time around 10 seconds for full chest coverage (Fig. 2.5). Such short acquisition time is critical for children, who are unable to accomplish long breath-holds (>10 seconds), especially if in respiratory distress [2].

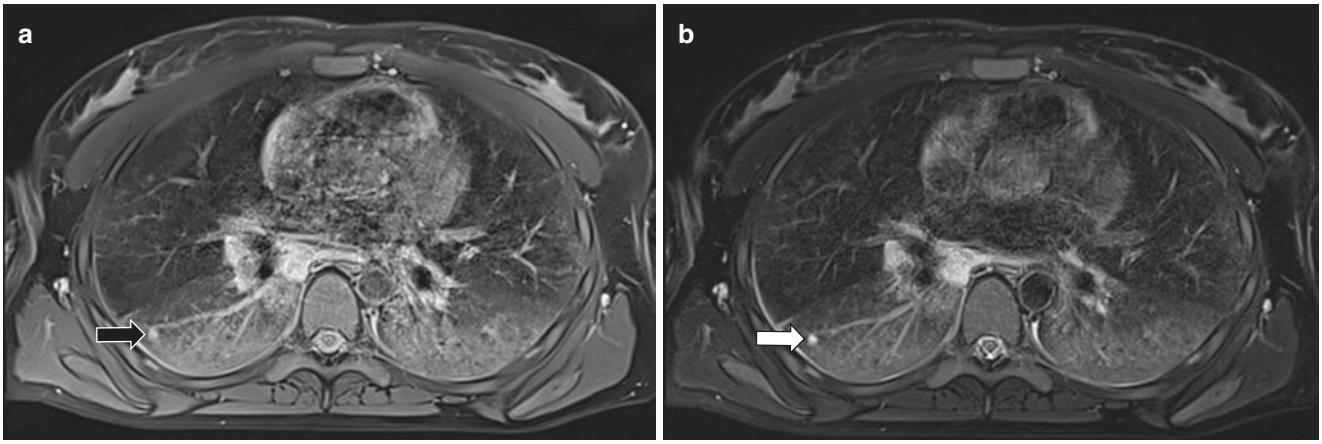

Fig. 2.4 Differing appearance of lungs and pulmonary nodule on black blood MR images in patient with systemic sclerosis. (**a**) Axial nonenhanced BLADE (Siemens) proton density-weighted MR image (1 × 1 × 5 mm, echo time of 28 ms) shows a nodule (*black arrow*) in the right lower lobe. (**b**) Axial nonenhanced BLADE (Siemens) T2-weighted MR image (1 × 1 × 5 mm, echo time of 87 ms) again shows the nodule (*white arrow*) in the right lower lobe which is more conspicuous than on the proton density-weighted MR image despite an overall lower signal-to-noise ratio on the T2-weighted MR image

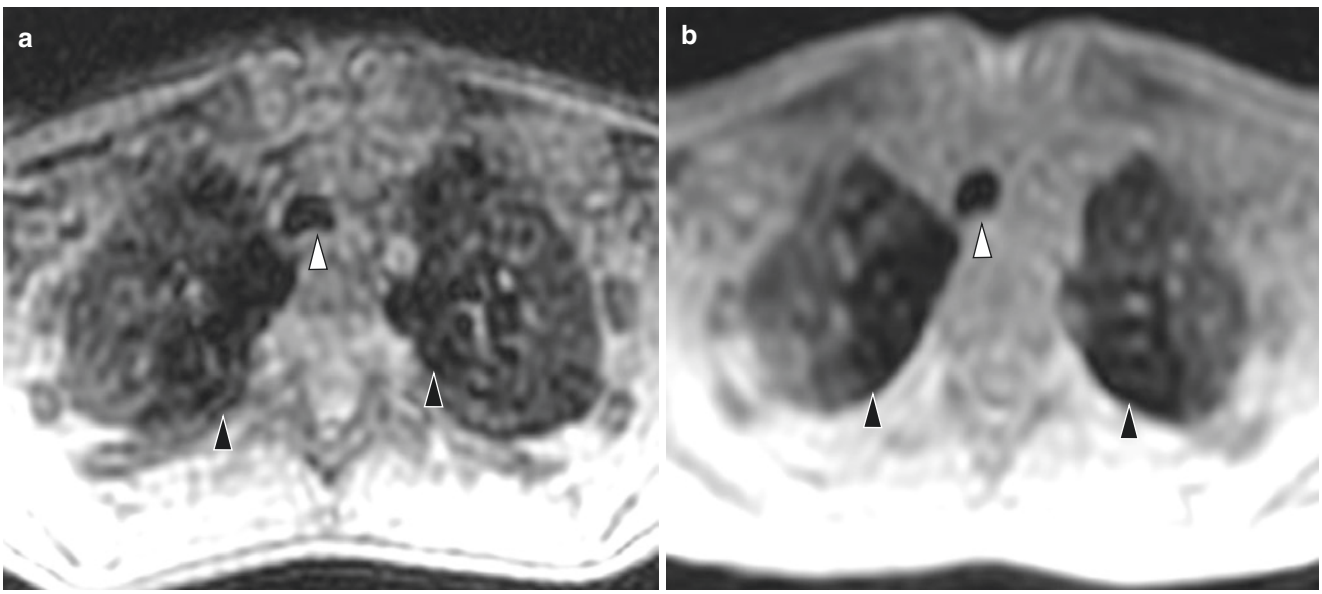

Fig. 2.5 Differing resolution of 3D SPGR MR imaging of the large airway. (**a**) Axial nonenhanced 3D SPGR MR image (2 mm isotropic voxel, echo time 0.7 ms) has higher noise and less definition of the trachea (*white arrowhead*) and less conspicuous air trapping (*black arrowheads*). (**b**) Axial nonenhanced 3D SPGR MR image (3 mm isotropic voxel, echo time 0.6 ms) has lower noise and higher signal-to-noise ratio, allowing for better definition of the trachea (*white arrowhead*) and more conspicuous air trapping (*black arrowheads*)

3D GRE acquisitions are usually preferred over 2D scans, because they can provide better SNR and are less sensitive to susceptibility artifacts [2]. The 3D dataset also enables multiplanar reformats (MPR), which allows for easy review of large airway pathology [2] (Fig. 2.6). For a fixed TR, GRE sequences provide contrasts ranging from proton-density-weighted (PD-weighted, using low flip angle readouts <3°) to T1-weighted (T1-weighted at higher flip angles). The PD-weighted setting is the most appropriate to assess large airways without the use of contrast agents, while the latter is used to assess vascular structures and lung parenchymal perfusion after contrast administration.

New variants of GRE with non-Cartesian k-space acquisition (helical) schemes have been developed to reduce sensitivity to motion artifacts [10, 11]. Cartesian geometry is inherently prone to motion-induced phase distortions, even if respiratory navigation or triggering techniques are used, which results in residual ghosting artifacts. The most promising alternative is the "radial" sampling scheme, which acquires the data along rotated spokes, or "stack of stars" (StarVIBE, Siemens, Munich, Germany) [12]. Due to overs-

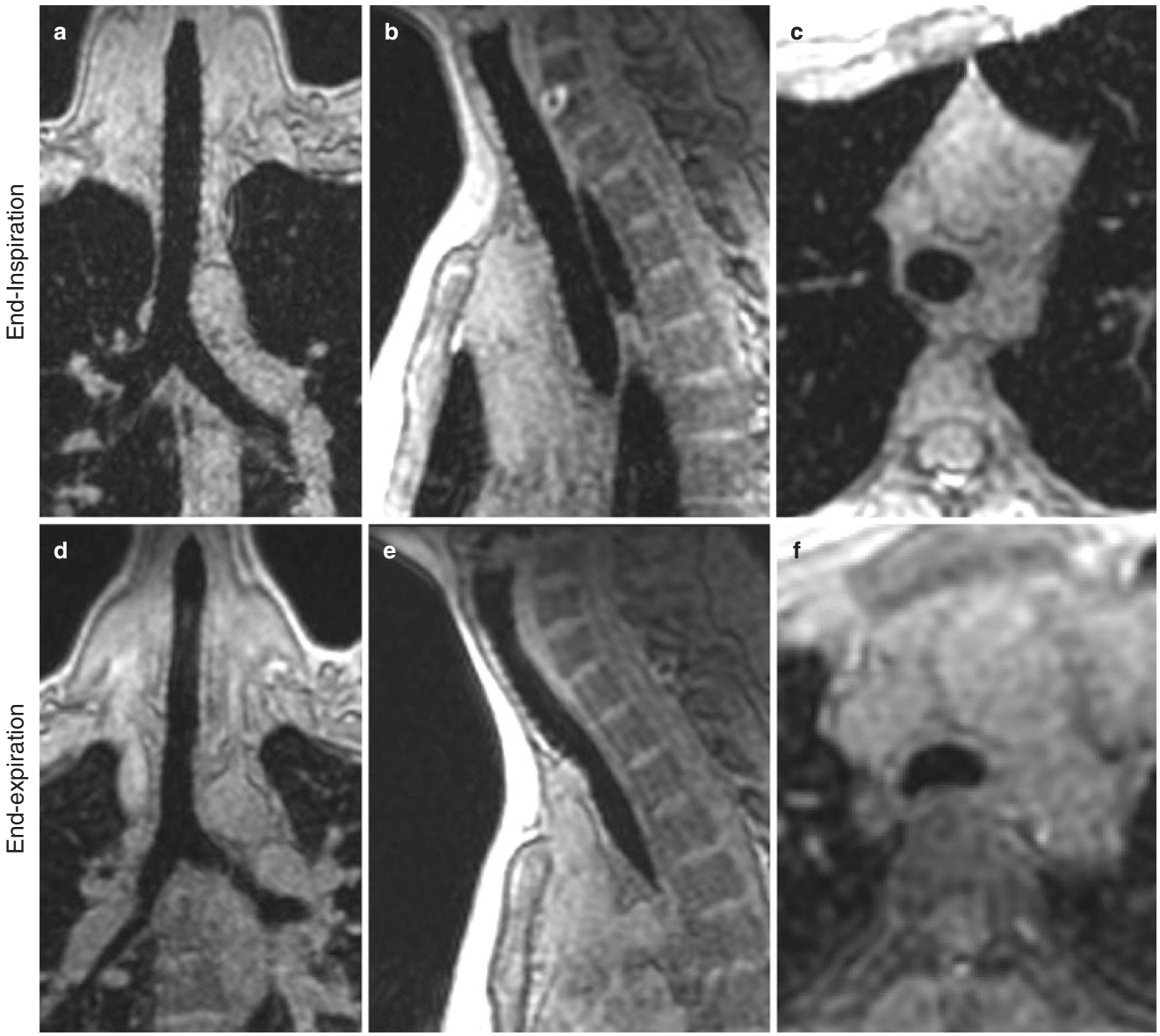

Fig. 2.6 Multiplanar reformatting (MPR) of end-inspiration and end-expiration spirometry gated 3D spoiled gradient echo (SPGR) in a 3.0 Tesla scanner on healthy subject. MR imaging acquired with a 32-channel cardiac array coil using a parallel imaging factor × 3, 12-sec acquisition time, and an isotropic voxel (2 × 2 × 2 mm). (**a**) Coronal nonenhanced 3D SPGR MR image obtained at end-inspiration. (**b**) Sagittal nonenhanced 3D SPGR MR image obtained at end-inspiration. (**c**) Axial nonenhanced 3D SPGR MR image obtained at end-inspiration. (**d**) Coronal nonenhanced 3D SPGR MR image obtained at end-expiration. (**e**) Sagittal nonenhanced 3D SPGR MR image obtained at end-expiration. (**f**) Axial nonenhanced 3D SPGR MR image obtained at end-expiration

ampling of the spokes in the center of the k-space, there is a reduction of ghosting artifacts because of a motion-averaging effect (similar to PROPELLER and BLADE scanning with FSE).

3D GRE sequences are usually combined with fat suppression techniques for large airway imaging. Fat suppression is important to cancel signal from mediastinal fat tissue, which surrounds the trachea, therefore highlighting the tracheal wall. Unfortunately fat suppression techniques may lead to signal loss in the trachea wall as well; therefore GRE two-point DIXON-based schemes are preferred to obtain homogeneous fat suppression (Fig. 2.7) [13].

Ultra-Short or Zero-TE (UTE/ZTE) Sequences UTE and ZTE are two variants of 3D GRE sequences with TE on the order of μs (microseconds) instead of ms (milliseconds). The shortening of TE allows minimization of the signal loss caused by $T2^*$ effects of air-tissue interfaces. k-space collection with UTE and ZTE can be performed both with radial or spiral trajectories achieving an oversampling of the center of the *k*-space [11, 14, 15]. This is desirable in large airway imaging because it reduces motion sensitivity. These sequences allow high SNR and sub-millimetric spatial resolution [11] (Fig. 2.8). UTE and ZTE are usually free-breathing acquisitions, which are combined with different respiratory triggering/gating

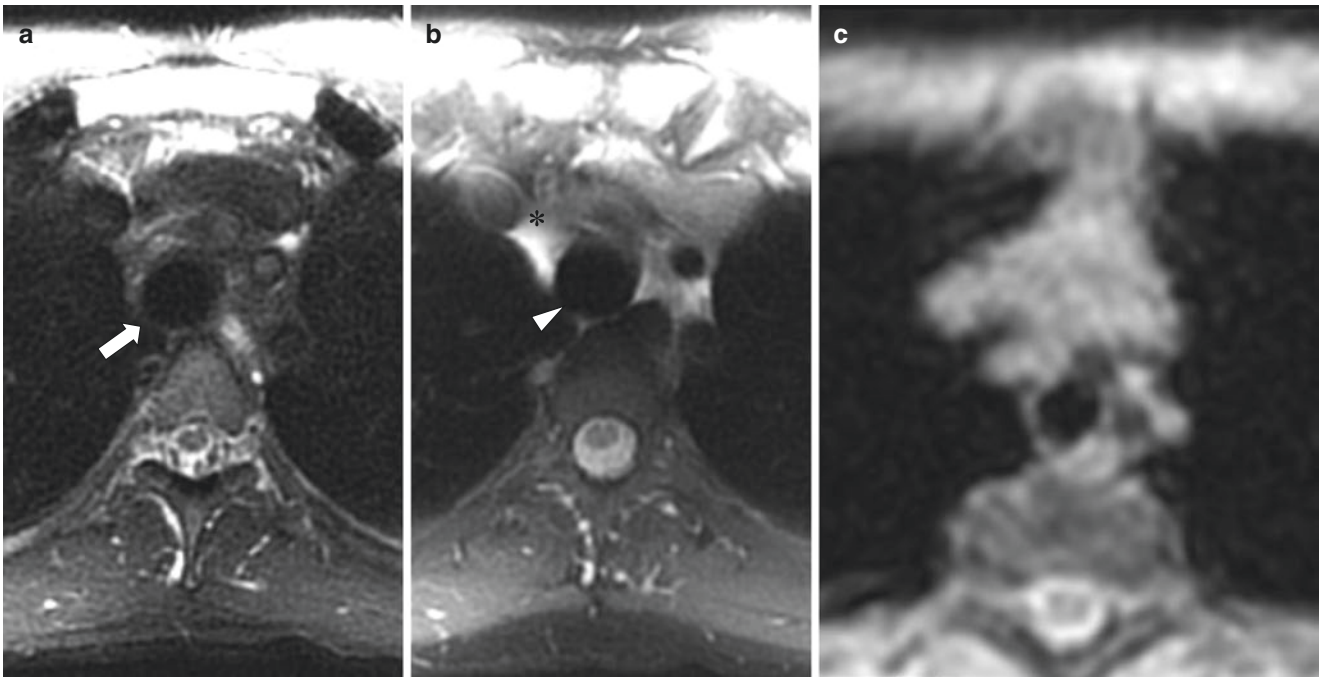

Fig. 2.7 Comparison of fat suppression techniques for large airway MR imaging. (**a**) Axial nonenhanced short tau inversion recovery (STIR) technique demonstrates generalized signal decay with reduced signal-to-noise ratio (SNR) of tracheal wall (*white arrow*). (**b**) Axial nonenhanced fat suppression technique (FATSAT) technique shows inhomogeneous fat signal cancellation with bright tissue in the anterior mediastinum (*) and low signal-to-noise ratio in the posterior tracheal wall (*arrowhead*). (**c**) Axial nonenhanced water map from two-point DIXON technique shows homogeneous SNR and fat cancellation

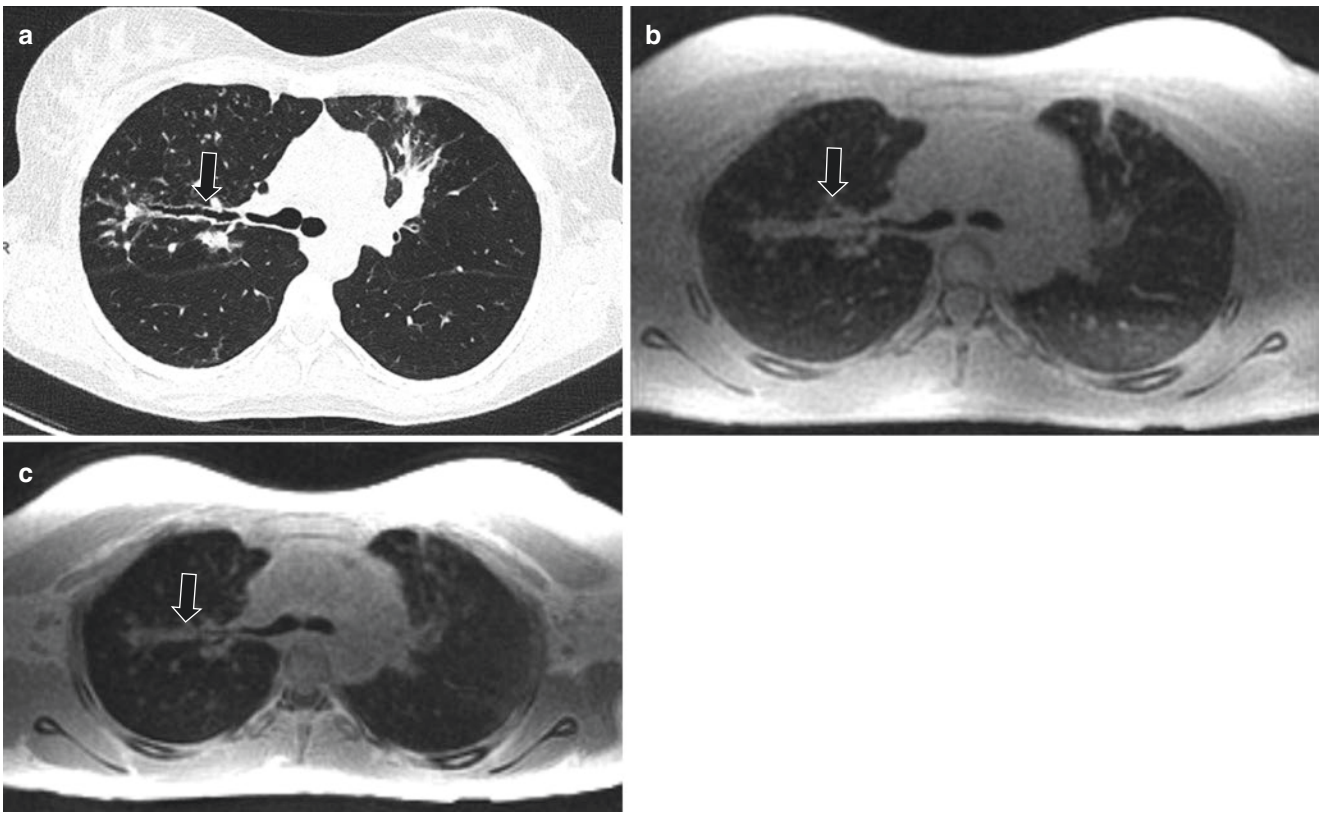

Fig. 2.8 Comparison of ultra-short echo time (UTE), zero echo time (ZTE), and CT for large airway MR imaging. (**a**) Axial nonenhanced lung window setting CT image obtained at end-expiration shows right upper lobe bronchiectasis and bronchial wall thickening (*black arrow*). (**b**) Axial nonenhanced free-breathing navigator-triggered zero echo time (ZTE) MR image obtained at end-expiration shows right upper lobe bronchiectasis and bronchial wall thickening (*black arrow*) with resolution approaching that of CT. (**c**) Axial nonenhanced pneumobelt-triggered ultra-short TE (UTE) MR image obtained at end-expiration shows right upper lobe bronchiectasis and bronchial wall thickening (*black arrow*) with resolution approaching that of CT

methods, such as prospective pneumobelt, or prospective and retrospective navigator-based echo scanning. The latter method was recently used in a group of infants to assess large airway collapse [16]. This method allows for acquisition of the images with free breathing and to retrospectively reconstruct the images in inspiration and expiration. Unfortunately respiratory gating requires long acquisition times, which can range between 6 and 15 minutes depending on the voxel size chosen (0.7–1.5 mm). Further refinements of these techniques might allow to achieve breath-hold acquisitions with spatial resolution more comparable to CT.

3D Fast Spin-Echo Sequences These are a family of 3D T2-weighted sequences that can provide isotropic resolution and allow multiplanar reformatted images with high SNR and CNR from the bronchial wall. These sequences have different acronyms according to the MR imaging vendors (CUBE, General Electric [GE], Boston, MA, USA; VISTA, or "Volume ISotropic Turbo spin echo Acquisition," Philips, Amsterdam, The Netherlands; and SPACE, or "Sampling Perfection with Application optimized Contrasts using different flip angle Evolution," Siemens) [2]. *k*-space acquisition schemes differ between vendors but they have some similar contrast and readout characteristics, using long echo train lengths, ultra-short echo spacings, and low flip readout angles in combination with parallel and partial Fourier imaging schemes to reduce acquisition time. These sequences can achieve isotropic voxel resolutions as low as 2 mm with free breathing in a reasonable imaging time (5–10 min) (Fig. 2.9).

Dynamic MR Large Airway Imaging

The high temporal resolution and the lack of radiation have made MR imaging suitable for studying airways in true dynamic conditions (cine-MR imaging). Cine-MR imaging can be performed both with 2D and 3D acquisitions [17]. The former includes sequences, such as 2D SSFP or 2D GRE, acquiring a single thick slice in a multiphase setting. Temporal resolution ranges between 100 and 200 ms per frame with a voxel resolution of 1 × 1 × 5 mm. A limitation of 2D imaging is that the trachea moves in all directions during the respiratory cycle; therefore a single slice could miss relevant airway

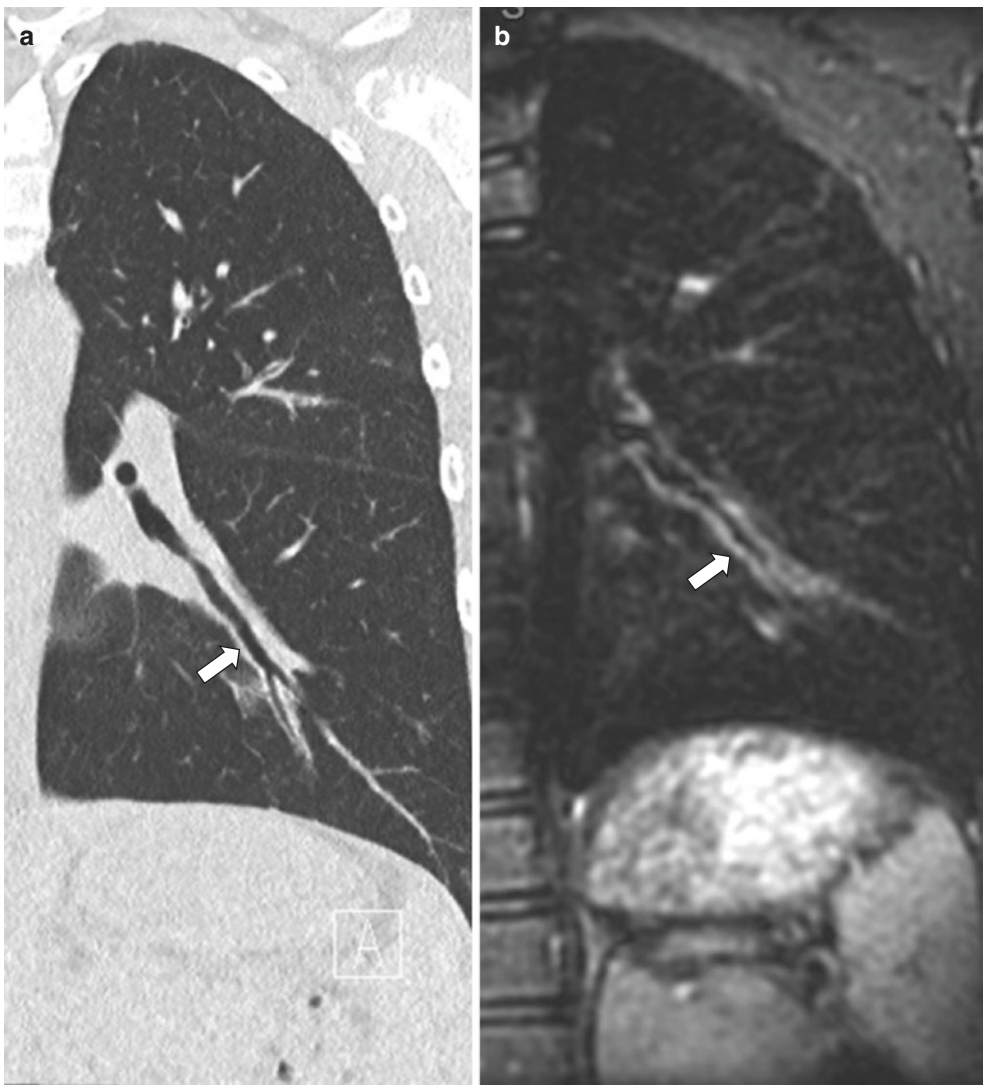

Fig. 2.9 Comparison of 3D T2-weighted MR imaging of the airway to CT in a pediatric patient with cystic fibrosis. (**a**) Coronal nonenhanced lung window setting CT image shows bronchiectasis and bronchial wall thickening (*arrow*) in left lower lobe. (**b**) Coronal nonenhanced isotropic three-dimensional (3D) CUBE (GE) T2-weighted MR image shows the bronchiectasis and bronchial wall thickening (*arrow*) resolution approaching that of CT

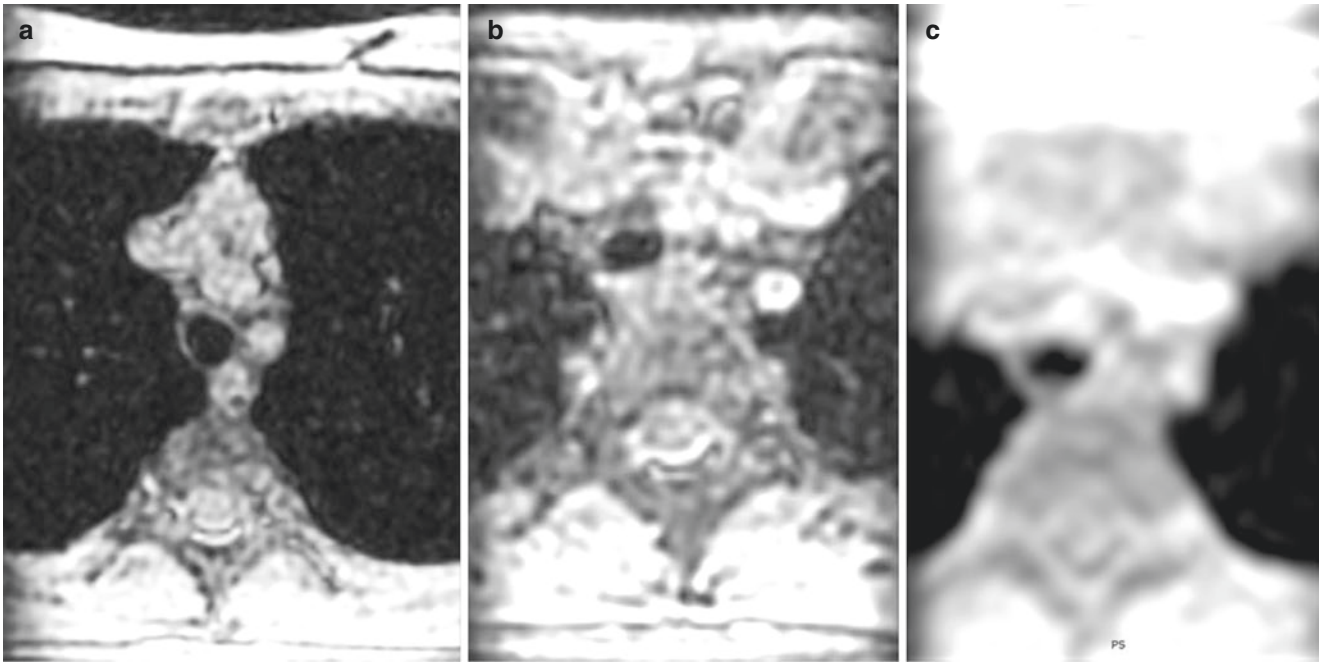

Fig. 2.10 Normal dynamic large airway MR imaging in a 12-year-old girl. (**a**) Axial nonenhanced 3D SPGR MR image obtained at end-inspiration shows a patent trachea. (**b**) Axial nonenhanced 3D SPGR MR image obtained at end-expiration shows a patent trachea which is slightly smaller than at end-inspiration, a normal finding. (**c**) Axial nonenhanced 3D SPGR MR image with *time-resolved imaging of contrast kinetics* (TRICKS) obtained during forced expiration shows a patent trachea which is slightly smaller than at end-inspiration, a normal finding

pathology during trachea movement. 3D cine-MR imaging includes 3D UTE sequence with retrospective reconstruction, previously mentioned, and 3D GRE sequences combined with keyhole imaging technique [16]. The latter includes sequences such as TRICKS, or "Time-Resolved Imaging of Contrast KineticS" (GE); DISCO, or "DIfferential Sub-sampling with Cartesian Ordering") (GE); TWIST, or "Time-resolved angiography With Interleaved Stochastic Trajectories") (Siemens); and D-TRAK, or "4D Time-Resolved Angiography using Keyhole" (Philips) [2]. These techniques allow temporal resolution in the order of 500 ms or less with isotropic voxel size between 2 and 3 mm (for a volume covering the large airways in a sagittal slab of approx. 9–12 cm). TRICKS cine-MR imaging was used to assess tracheobronchomalacia in a group of pediatric patients [18], showing that cine-MR imaging is a possible alternative to bronchoscopy and cine-CT for tracheobronchomalacia [19] (Fig. 2.10).

Anatomy

Embryology

The respiratory diverticulum starts as an outgrowth from the ventral part of the foregut around 4 weeks of gestation. The respiratory diverticulum originates from the endodermal layer, and it forms the epithelium of the larynx, trachea, and bronchi, as well as that of the lungs [20, 21]. The cartilaginous, muscular, and connective tissue components of the trachea and lungs are derived from the mesoderm layer of the foregut. Initially, the respiratory diverticulum is in open communication with the foregut [22]. When the diverticulum expands caudally, two longitudinal ridges, the tracheoesophageal ridges, separate it from the foregut [22]. Afterward, these ridges fuse to form the tracheoesophageal septum, which divides the foregut into a dorsal portion, the esophagus, and a ventral portion, the trachea and lung.

The lung bud then divides into right and left primary bronchial buds. Three main branches form in the right lung bud and two in the left. These initial branches correspond to the lobar bronchi of the adult lungs. The lung grows caudally and laterally, entering the pericardio-peritoneal layers [23]. At 9 weeks' gestation the pleura separates from the pericardium and peritoneum developing the visceral pleura, which covers the lung, and the parietal pleura, which covers the chest wall and diaphragm. The pattern of airway branching is complete by about the 16th week of intrauterine life [23]. Any interruption of these steps of the embryological formation (Fig. 2.11) results in tracheobronchial branching anomalies.

Normal Development and Anatomy

Although airway size changes after birth, the pattern of branching does not. Therefore, a newborn has essentially the same airway structure as an adult, but in miniature.

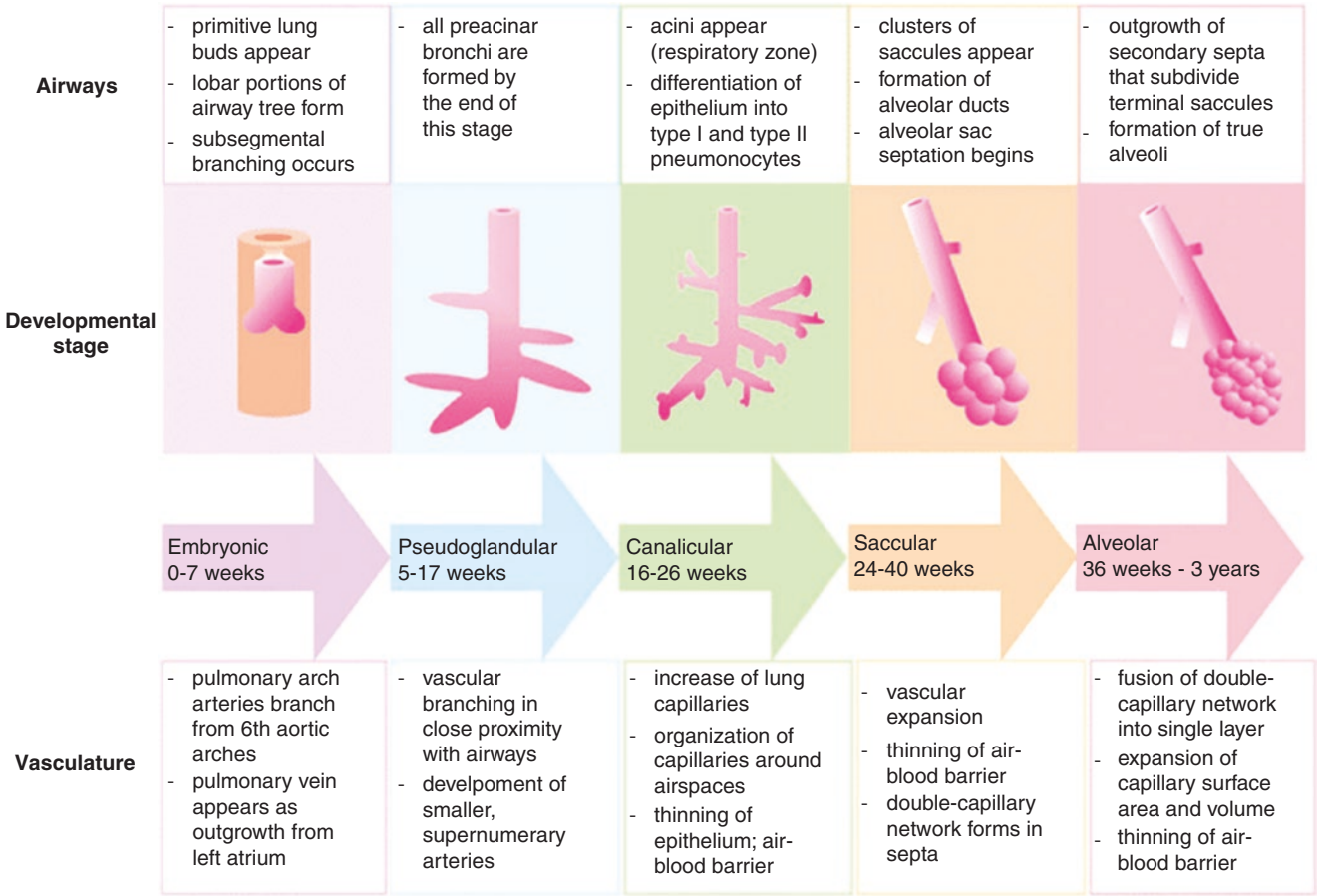

Fig. 2.11 Diagram illustrating normal lung development: airway structure and pulmonary vasculature

After birth, airways will keep growing until adulthood with a final diameter and length double or triple of that at birth [21, 24, 25].

In the parlance of the pathologist, the large airways include those airways extending from the mouth to the respiratory bronchiole [26]. Conversely, in the parlance of a radiologist, large airways are those airways that are visible on CT imaging, which include airways extending down to the segmental bronchi [27, 28]. Radiologists further divide large airways into upper and lower airways, where the upper airway extends from the mouth to the trachea, including the pharynx and the larynx [29].

The pharynx is a tubular structure, which connects the posterior nasal and oral cavities to the larynx and esophagus. It is divided into nasopharynx, oropharynx, and laryngopharynx. The larynx is a moving structure containing cartilage, muscles, and ligaments. The larynx performs various functions, including phonation and airway protection.

The trachea begins inferior to the cricoid cartilage of the larynx and it extends to the carina at the level of the fifth thoracic vertebra [27, 30] (Fig. 2.12). Trachea length varies between 10 and 15 cm in adults according to gender and patient length, and it contains 16–20 C-shaped cartilaginous rings open posteriorly at level of the pars membranacea, that is, the posterior wall of the trachea formed by the trachealis muscles [30]. The trachea is in the midline of the thorax and it is slightly displaced to the right by the aortic arch. The trachea bifurcates into the right and left main bronchi at the carina. The right main bronchus is more vertically positioned than the left main bronchus, resulting in a greater likelihood of foreign body aspiration or endotracheal tube entering the right bronchial lumen. Main bronchi are further divided in lobar bronchi (two on the left and three on the right), which supply each of the main lobes of the lung (upper, middle, and lower lobe on the right and upper and lower on the left side). Segmental bronchi supply each bronchopulmonary segment of the lungs [27, 30].

Anatomic Variants

Branching Anomalies

Branching anomalies depend on the embryological phase at which they occurred. A summary of the branching anomalies according to a classification based on anatomical, embryological, and functional criteria is shown in Table 2.2.

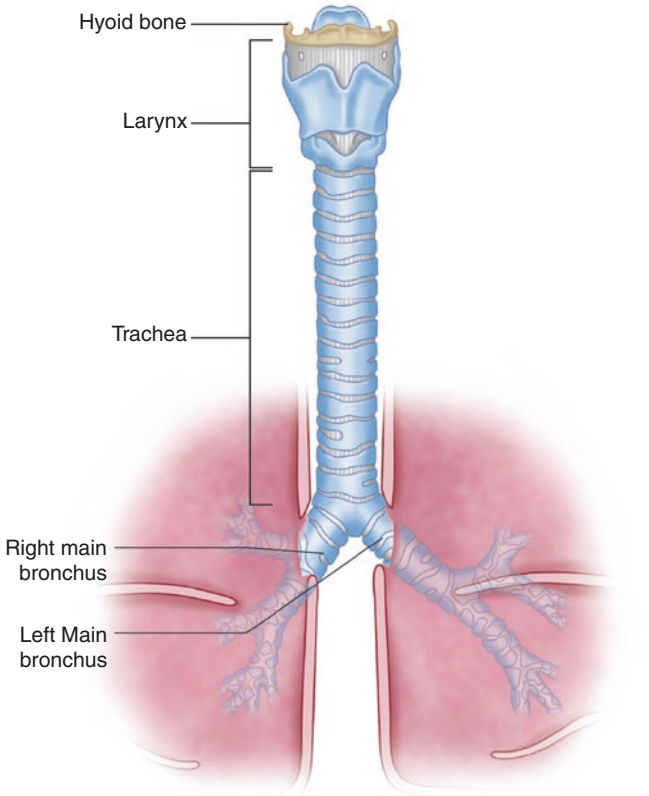

Fig. 2.12 Anatomy of the trachea

Table 2.2 Airway branching and developmental anomalies

Developmental or anatomical defect	Resulting condition
Interruption of normal development	Agenesis-hypoplasia complex
Obstruction or compression	Tracheal stenosis Bronchial atresia Tracheal dilatation (Mounier-Kuhn syndrome)
Bronchopulmonary malformation of the foregut	Tracheoesophageal fistula Esophageal bronchus Bronchogenic cyst
Ectopic or supernumerary	Tracheal bronchus Accessory cardiac bronchus Tracheobronchial diverticulum
Malformation associated with situs anomalies	Situs inversus Heterotaxia

Tracheal Stenosis

Congenital tracheal stenosis is a rare condition characterized by a reduction of the tracheobronchial luminal diameter, usually greater than 50% [31]. The narrowing can be focal or generalized and may be associated with cartilaginous rings (isolated form) or compression by an extrinsic structure such as a vascular anomaly or congenital cyst [31]. Tracheal stenosis is frequently misdiagnosed as refractory asthma, causing delayed diagnosis in many cases [32]. When tracheal narrowing is diagnosed, congenital tracheal stenosis is a diagnosis of exclusion, when other possible etiologies such as inflammatory, traumatic, neoplastic, or iatrogenic causes of airway narrowing have been excluded.

Although CT is a current imaging modality of choice for evaluating congenital tracheal stenosis, MR imaging can be used instead and it can also demonstrate associated anomalies such as vascular malformations. On MR imaging, fixed tracheal narrowing throughout the respiratory cycle is seen in affected pediatric patients. Although axial MR imaging may be sufficient for demonstrating the degree of tracheal stenosis, the overall length of tracheal stenosis is best seen on sagittal MR imaging.

In symptomatic pediatric patients with congenital tracheal stenosis, surgical correction is currently the management of choice. While short-segment tracheal stenosis (≤5 cm) is treated with end-to-end anastomosis, patch or tracheal autograft repair is often used for long-segment tracheal stenosis. Another newer option is slide tracheoplasty, which is known to be associated with less risks of developing stricture and granulation tissue formation. Treatment result can be efficiently evaluated with MR imaging to assess post-surgical changes and residual or recurrent stenosis (Fig. 2.13).

Heterotaxy

Heterotaxies are anomalies related to the abnormal position of the organs in the thorax or abdominal cavity. Normal position of the organs (situs solitus) includes a left-sided heart and right-sided liver [33]. A mirror image of the normal organ disposition with a right-sided heart (dextrocardia) and left-sided liver is known as situs inversus. Situs inversus can be associated with congenital heart disease and primary ciliary dyskinesia (PCD). The triad of situs inversus, PCD, and chronic sinusitis (± nasal polyposis) is known as Kartagener syndrome. Situs ambiguus (heterotaxy) is an anomaly in the normal left and right distribution of the thoracic and abdominal organs which does not match the configuration of a situs inversus. A typical feature of situs ambiguus is the symmetrical and identical configuration of the bronchial tree and lung, from which derives the term isomerism [34].

In right isomerism, both lungs are trilobed with bilateral minor fissures, associated asplenia, midline positioning of the liver and stomach, intestinal malrotation, and severe cardiac anomalies. Right isomerism usually presents early due to associated congenital cyanotic heart disease and asymptomatic cases discovered in adulthood are rare (<1%) [34, 35]. In left isomerism, both lungs are bilobed, there is no minor fissure, and the main bronchi are elongated. Left isomerism is associated with midline positioning of liver and multiple small splenules, defined as polysplenia in almost half of the cases [35]. Left isomerism can be associated with intestinal malrotation and with azygos continuation of the inferior vena cava (IVC), which consist of absence of the hepatic

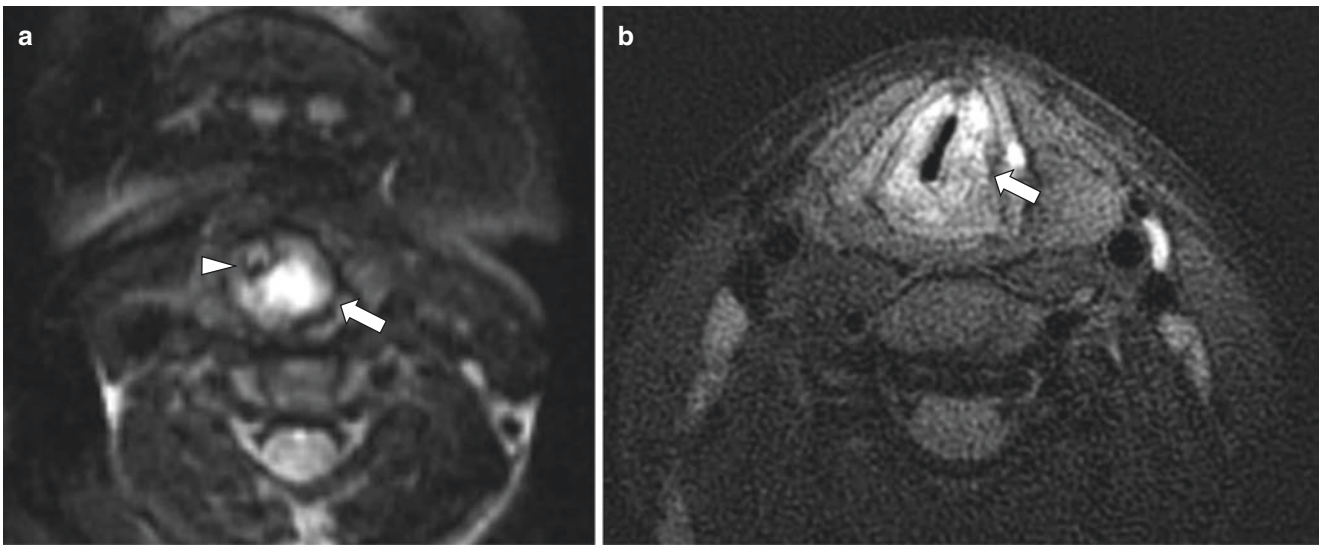

Fig. 2.13 Congenital laryngeal stenosis from a laryngeal cyst in a 1-year-old girl. (**a**) Axial nonenhanced T2-weighted fast spin-echo MR image shows a hyperintense cyst (*arrow*) in the left side of the larynx causing luminal stenosis (*arrowhead*). (**b**) Axial nonenhanced T2-weighted PROPELLER MR image obtained after resection shows thickening and deviation of the left vocal cords (*arrow*). Post operative imaging was performed when patient was 14-years-old

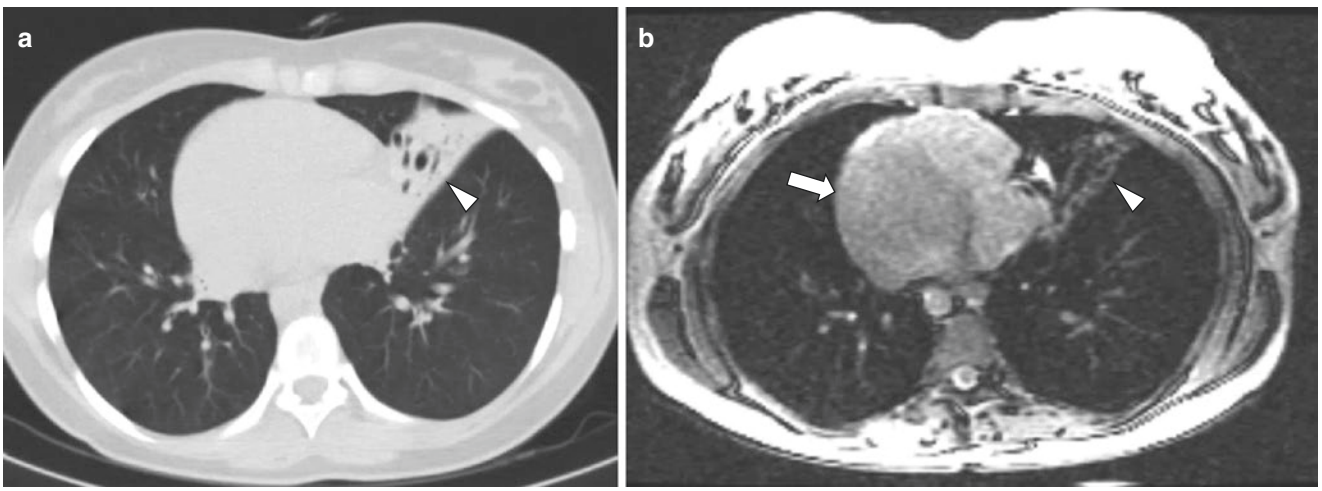

Fig. 2.14 Primary ciliary dyskinesia in a 17-year-old girl with situs inversus. (**a**) Axial nonenhanced lung window setting CT image obtained at end expiration shows dextrocardia and an area of consolidation with bronchiectasis (*arrowhead*) in the left-sided middle lobe. (**b**) Axial nonenhanced SSFP MR image shows dextrocardia with a right-sided left ventricle (*arrow*) and an area of consolidation with bronchiectasis (*arrowhead*) in the left-sided middle lobe

segment of the IVC with venous drainage of the lower half of the body via a dilated azygos vein. Cardiac abnormalities are less common in left isomerism than right isomerism, and left isomerism is more frequently asymptomatic.

Although CT is the most often used technique to assess airway pathology and associated cardiac anomalies, MR imaging can be used as an alternative, offering the benefit of cinematic assessment of large airways and cardiac physiology and pathology. In patients with situs inversus and PCD, lung pathology can be assessed with MR imaging showing typical imaging findings of dextrocardia, middle lobe consolidation, and bronchiectasis (Fig. 2.14).

In this group of patients, treatment is focused on repairing congenital heart defects (when present) and treating lung disease related to PCD. PCD treatment is mostly medical and lobectomy is not routinely suggested as therapy in PCD [36].

Spectrum of Large Airway Disorders

Congenital Large Airway Disorders

Macroglossia

Macroglossia refers to a tongue which protrudes beyond the alveolar ridge [37]. It may occur due to a focal mass or diffuse enlargement, which is associated with several genetic syndromes. Whether macroglossia is due to a focal mass or diffuse enlargement, both may lead to tongue dysfunction

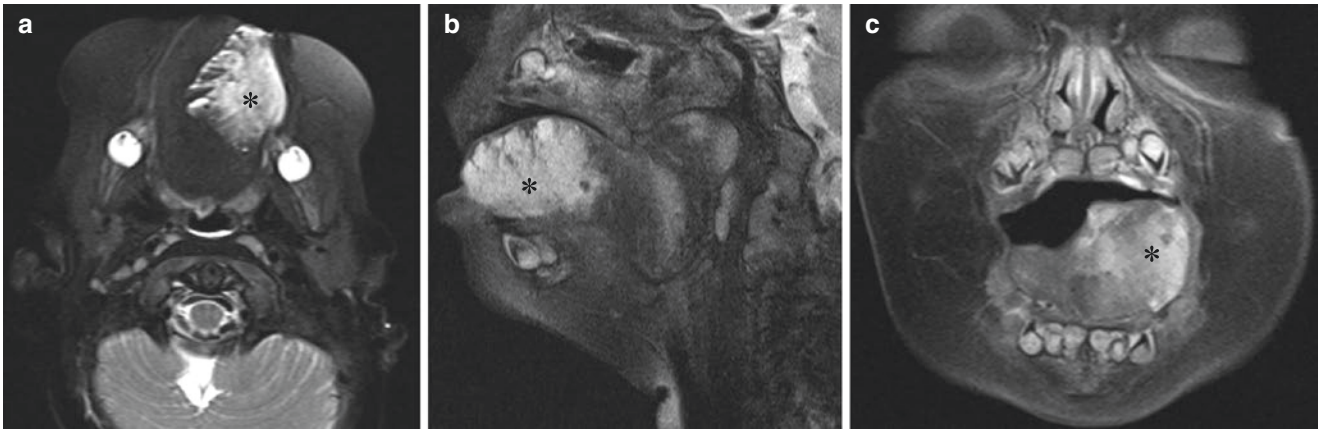

Fig. 2.15 Macroglossia due to blue rubber bleb nevus syndrome in a 5-month-old girl who presented with respiratory distress. (**a**) Axial nonenhanced T2-weighted MR image with fat suppression shows hyperintense lesion (*) in the left side of the tongue. (**b**) Sagittal nonenhanced T2-weighted MR image with fat suppression shows hyperintense lesion (*) within the tongue. (**c**) Coronal nonenhanced T2-weighted MR image with fat suppression shows hyperintense lesion (*) in the left side of the tongue

including alterations in chewing and speech and airway obstruction. Diffuse enlargement of the tongue may occur in Beckwith-Wiedemann syndrome (BWS), congenital hypothyroidism, chromosomal abnormalities, hemi-hyperplasia, and mucopolysaccharidoses (i.e., Pompe disease). Relative macroglossia is also seen in Down syndrome, micrognathia, muscular hypotonia, and angioedema. Macroglossia can also occur in cases of tissue infiltration as in case of neoplasms, neurofibromatosis, inflammatory and infectious causes, lymphatic or venous malformations (i.e., blue rubber bleb nevus syndrome), and hemangiomas. Affected pediatric patients with vascular anomalies of the tongue may present with varying symptoms depending on the size and extent of the lesion, including obstructive symptoms or recurrent bleeding.

Although CT with and without intravenous contrast is the primary imaging modality used for the evaluation of macroglossia, it has the disadvantage of requiring ionizing radiation [37]. MR imaging is an excellent alternative to CT in these cases, since it offers excellent depiction of vascular structures without the need for ionizing radiation. Angiographic MR imaging can depict the course of any abnormal vessels and provide for pre-therapeutic planning [38]. MR imaging has the added advantage of characterizing lesions in multiple sequences, often allowing for better diagnostic accuracy. For example, in a pediatric patient with macroglossia due to vascular anomalies, high-flow lesions show signal flow voids both in T1-weighted and T2-weighted images, and low-flow lesions are characterized by low signal in T1-weighted and moderately homogeneous signal in T2-weighted images (Fig. 2.15).

Whenever possible, macroglossia is managed with medical treatment, which consists of conservative measures to reduce tongue inflammation and bleeding. In cases of severe airway obstruction and/or dysphagia from macroglossia, surgical procedures are performed to reduce tongue size while maintaining tongue mobility and function [39].

Tonsillar Hypertrophy

Tonsillar hypertrophy refers to the enlargement of the lymphoid tissue located in the wall of the pharynx including the adenoids and palatine and lingual tonsils [40]. These structures are part of the immune system of the upper airways, where the first response to infectious agents takes place. In cases of repeated infection or chronic colonization (mostly by *Staphylococcus* and *Streptococcus* family organisms), these structures can become hypertrophic, limiting airflow both at the level of nasopharynx (adenoid) and oropharynx (palatine tonsils). Typical clinical findings are nasal congestion, recurrent otitis, and obstructive sleep apnea syndrome (OSAS).

Although radiographic evaluation with a lateral neck radiograph is frequently performed for assessing tonsillar hypertrophy, this technique is not a reliable method for measuring the grade of obstruction [41]. CT can demonstrate lateral or anterior-posterior narrowing of the airway with much better anatomical detail. CT is highly useful for identifying upper airway obstruction and to develop an appropriate surgical plan. For this indication, CT can be performed in supine position and in different phases of respiration to provide information about airway cross-sectional area and site of obstruction. However, CT is limited by radiation exposure risk and imaging is typically performed in a single phase of respiration. In contrast, specialized MR imaging allows both static and dynamic imaging without exposing children to increased radiation [42, 43]. MR imaging measurements of tonsillar hypertrophy show good correlation with endoscopic assessment. If lingual tonsils are greater than 10 mm in diameter and abutting both the posterior border of the tongue and the posterior pharyngeal wall, they are considered markedly enlarged (Fig. 2.16). Adenoid enlargement is diagnosed if adenoid tissue is thicker than 12 mm and if there is intermittent obstruction of the posterior nasopharynx on sagittal cine-MR imaging.

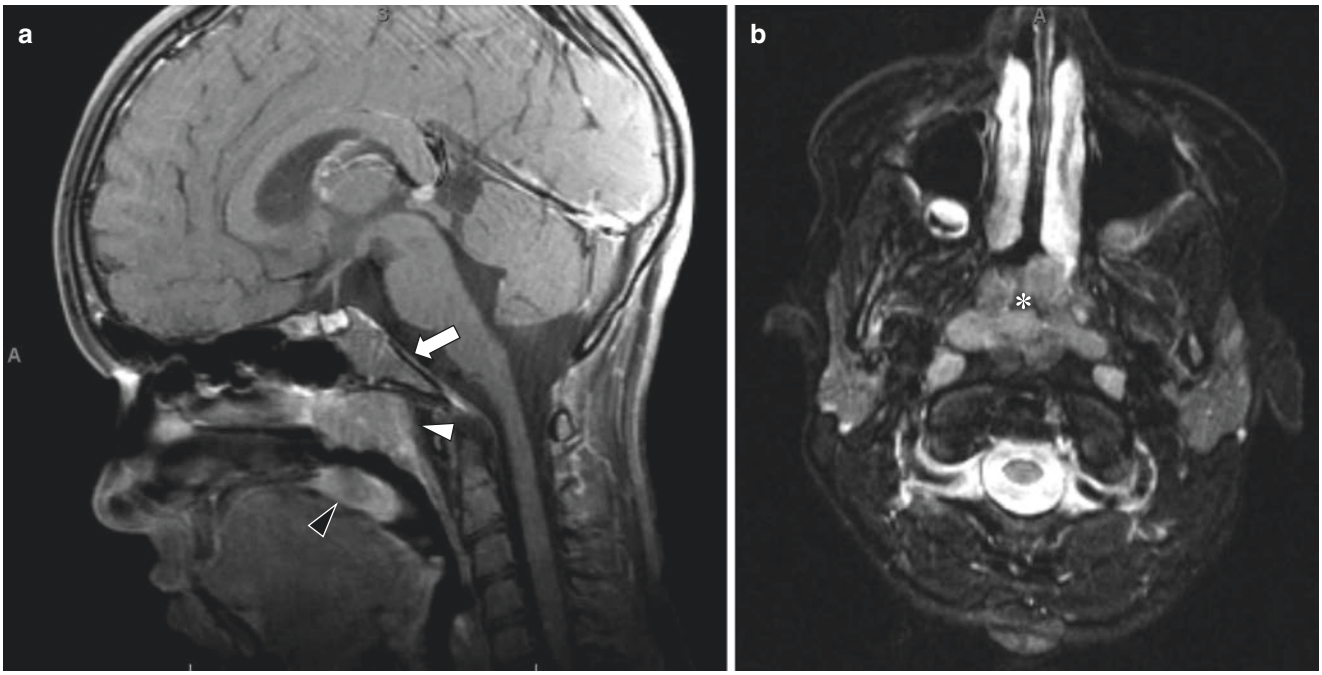

Fig. 2.16 Tonsil and adenoid hypertrophy in a 9-year-old girl who presented with breathing difficulty. (**a**) Sagittal enhanced T1-weighted MR image with fat suppression shows marked enlargement of adenoid (*arrow*), palatine tonsils (*white arrowhead*), and lingual tonsil (*black arrowhead*). (**b**) Axial enhanced T1-weighted MR image with fat suppression shows upper airway obstruction (*)

Tonsillectomy and adenoidectomy are often performed in children with chronic symptoms from tonsillar hypertrophy. Both procedures aim to improve airflow in the upper airways and to reduce recurrent infections.

Laryngeal Stenosis

Laryngeal stenosis is one of the most common causes of airway obstruction in infants and children. Laryngeal stenosis can be congenital or acquired. Acquired laryngeal stenosis is more common and is most often related to prolonged intubation. Congenital causes of laryngeal stenosis include glottic obstruction due to vocal cord thickening, congenital vocal cord paralysis due to nervous system disorders (e.g., Arnold-Chiari, hydrocephalus), laryngeal webs, congenital laryngeal cyst, and laryngomalacia [44]. Symptoms of congenital and acquired laryngeal stenosis are similar and may include stridor, dyspnea, and hypoxia [45].

Although direct visualization with endoscopy is the gold standard for diagnosis of laryngeal stenosis, radiologic evaluation plays an important role in most patients. Chest radiograph often helps to evaluate for secondary findings including atelectasis and pneumonia. CT can provide detailed anatomic information regarding the location and extension of the laryngeal stenosis; however, it often cannot differentiate between the true lumen and overlying secretions. In contrast, MR imaging can often make this differentiation due to better soft tissue characterization capability. MR imaging also has the benefit of producing cross-sectional anatomic information without the use of ionizing radiation [45].

Treatment of laryngeal stenosis usually requires surgical intervention such as laryngotracheal reconstruction with cricoid split using cartilage graft (Fig. 2.17) [45].

Congenital High Airway Obstruction Sequence

Congenital high airway obstruction sequence (CHAOS) is a rare congenital anomaly, characterized by obstruction of the fetal upper airway, including laryngeal atresia, stenosis or laryngeal cysts, and tracheal atresia or stenosis [46, 47]. The obstructed airway results in decreased clearance of the fetal lung fluid with increased intra-tracheal and lung pressure. Consequently, the lungs expand to abnormally large volumes leading to compression of mediastinal structures including the heart causing decreased venous return and hydrops [47]. CHAOS is commonly associated with genetic disorders such as Fraser's syndrome, a rare congenital syndromic anomaly characterized by tracheal/laryngeal atresia and facial and skeletal abnormalities [46].

Diagnosis is usually made prenatally by ultrasound with detection of CHAOS abnormalities around the 20th week of gestation or earlier. On prenatal ultrasound, typical signs of CHAOS are enlarged symmetrical hyper-echogenic lungs with flattening or inversion of the diaphragm [47]. The airway is dilated up to the level of the obstruction. The heart and mediastinum appear small and anteriorly displaced by the enlarged lungs. On prenatal MR imaging, the lungs are enlarged and hyperintense with flattening or inversion of the diaphragm and mediastinal displacement [48]. Compared to ultrasound, MR imaging can often better identify the level of airway obstruction due to a higher soft tissue characteriza-

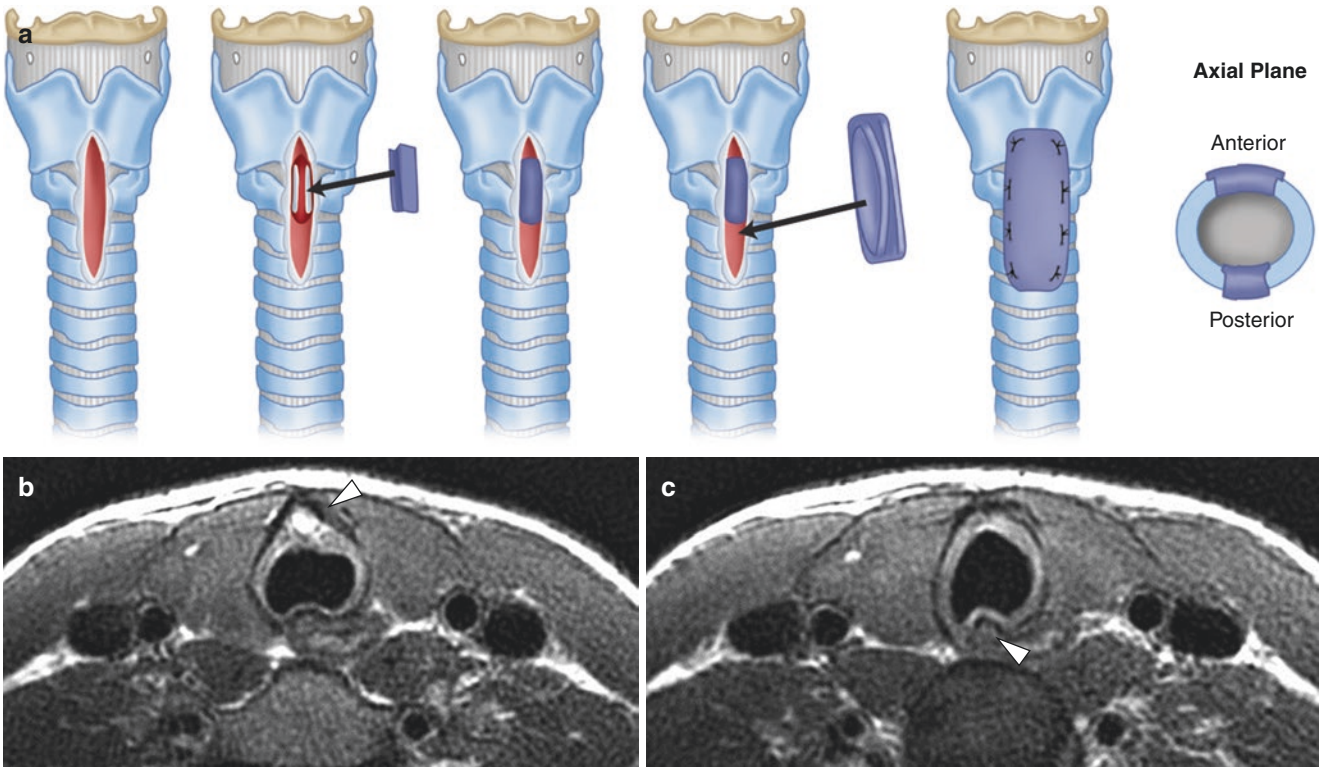

Fig. 2.17 Laryngeal stenosis treated with laryngotracheal reconstruction with cricoid split using cartilage graft in a 12-year-old boy. (**a**) Illustration of surgical procedure of anterior and posterior cricoid split with costal cartilage graft, where cricoid is opened anteriorly and posteriorly and two cartilage grafts are positioned to enlarge cricoid lumen. (**b**) Axial nonenhanced T2-weighted PROPELLER MR image shows the anterior graft (*arrowhead*). (**c**) Axial nonenhanced T2-weighted PROPELLER MR image shows the posterior graft (*arrowhead*)

tion and 3D capabilities [48]. Differential diagnosis of CHAOS includes causes of extrinsic compression of the airways, such as lymphatic malformation, cervical teratoma, and vascular abnormalities (Fig. 2.18).

Large series show that CHAOS is highly lethal, with occasional reports of survivors after direct postnatal surgical intervention to the upper airways [46].

Tracheoesophageal Fistula

Tracheoesophageal fistula (TEF) consists of a fistulous connection between the esophagus and trachea, often with associated esophageal atresia [49]. Congenital TEF has an incidence of 1 in 3500 births. It may be associated with other congenital abnormalities, including cardiac anomalies, VACTERL (Vertebral defects, Anal atresia, Cardiac defects, Tracheo-Esophageal fistula, Renal anomalies, and Limb abnormalities) syndrome, and gastrointestinal anomalies (e.g., malrotation, intestinal atresia) [49]. TEF and esophageal atresia are classified in five types: (1) isolated esophageal atresia without TEF (type A), (2) proximal tracheoesophageal fistula with distal esophageal atresia (type B), (3) proximal esophageal atresia with distal fistula (type C, the most frequent type), (4) double fistula with intervening esophageal atresia (type D), and (5) isolated fistula (type H) [49, 50]. Typical symptoms of TEF are coughing, choking or cyanosis during feeding, vomiting, and dyspnea.

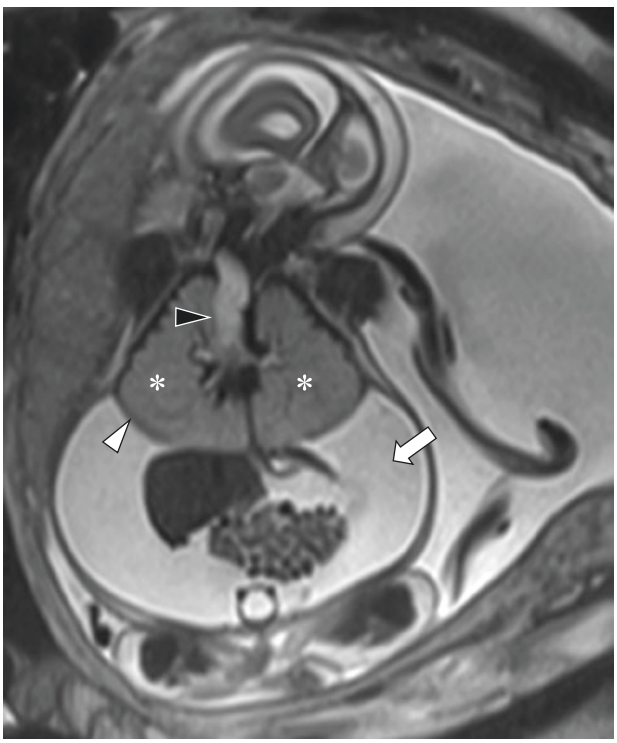

Fig. 2.18 Congenital high airway obstruction sequence (CHAOS) in a male fetus at 27 weeks' gestation. Coronal nonenhanced T2-weighted HASTE MR image shows enlarged hyperintense lungs (*), dilated central airways (*black arrowhead*), inversion of the diaphragm (*white arrowhead*), and ascites (*arrow*)

TEF is usually first suspected based on prenatal ultrasound findings, which may include polyhydramnios, non-visualized stomach, and distended upper esophagus. Prenatal MR imaging may be subsequently performed and has been shown to have high sensitivity and specificity for the prenatal diagnosis of TEF [51, 52]. MR imaging is also an excellent tool to assess for tracheomalacia, a common complication of TEF which is described in the following sections [53] (Fig. 2.19).

TEF is treated surgically with fistula ligation and creation of a primary esophageal anastomosis. When primary anastomosis is not possible due to a long-gap esophageal atresia, a staged repair may be performed after esophageal elongation, colonic interposition graft may be utilized, or gastric pull-up may be performed [53].

Ectopic Bronchus: Tracheal Bronchus

A tracheal bronchus (TB) is an anomalous bronchus that originates directly from the trachea or the main bronchus, usually located from 6 cm above the carina up to 2 cm below [23, 54, 55]. These bronchi can be considered as normal "displaced" bronchi or supernumerary bronchi [55]. They are considered supernumerary when they coexist with a normal segmentation of the bronchial tree. In contrast, they are considered displaced when a segmental bronchus is missing from its usual normal division for a lobe. Other two possible variants are the rudimentary and anomalous TB, where the former is a blind outpouching on the right lower side of the trachea and the latter arises above the tracheal bifurcation and contains three normal bronchial segments (Fig. 2.20). TB is more frequently seen on the right side and in the upper lobes. The most common variant is the displaced TB extending to the right upper lobe [55], which is also the most frequent congenital anomaly of the tracheobronchial tree overall [56]. TB is usually asymptomatic, although symptoms are more frequently present in left-sided TB and in the supernumerary form. Cough and recurrent infection are two most commonly encountered symptoms in patients with TB [55, 56].

Although the most used technique to diagnose TB remains CT, MR imaging can provide similar diagnostic capability without the need for potentially harmful ionizing radiation. On MR imaging, a TB is seen as a small tubular structure

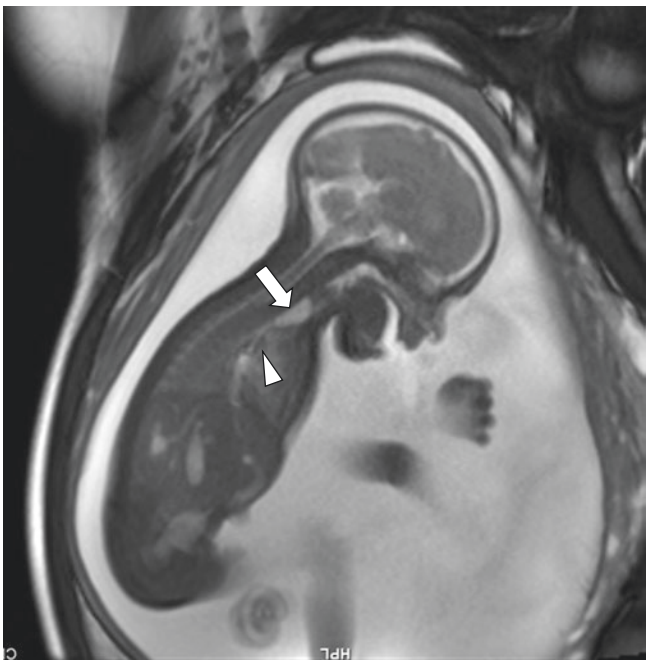

Fig. 2.19 Male fetus at 28 weeks' gestation with esophageal atresia with tracheoesophageal fistula. Sagittal T2-weighted SSFSE/HASTE MR image shows dilatation of proximal esophagus (*arrow*) with connection to the bronchial tree (*arrowhead*)

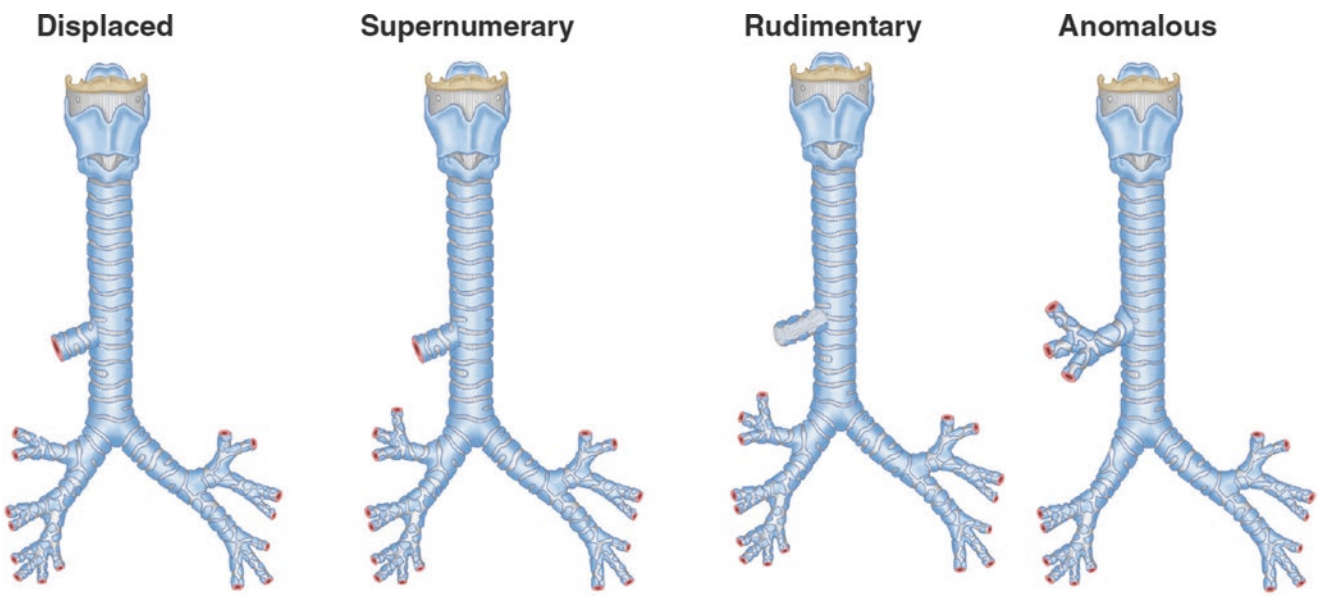

Fig. 2.20 Variation of tracheal bronchus

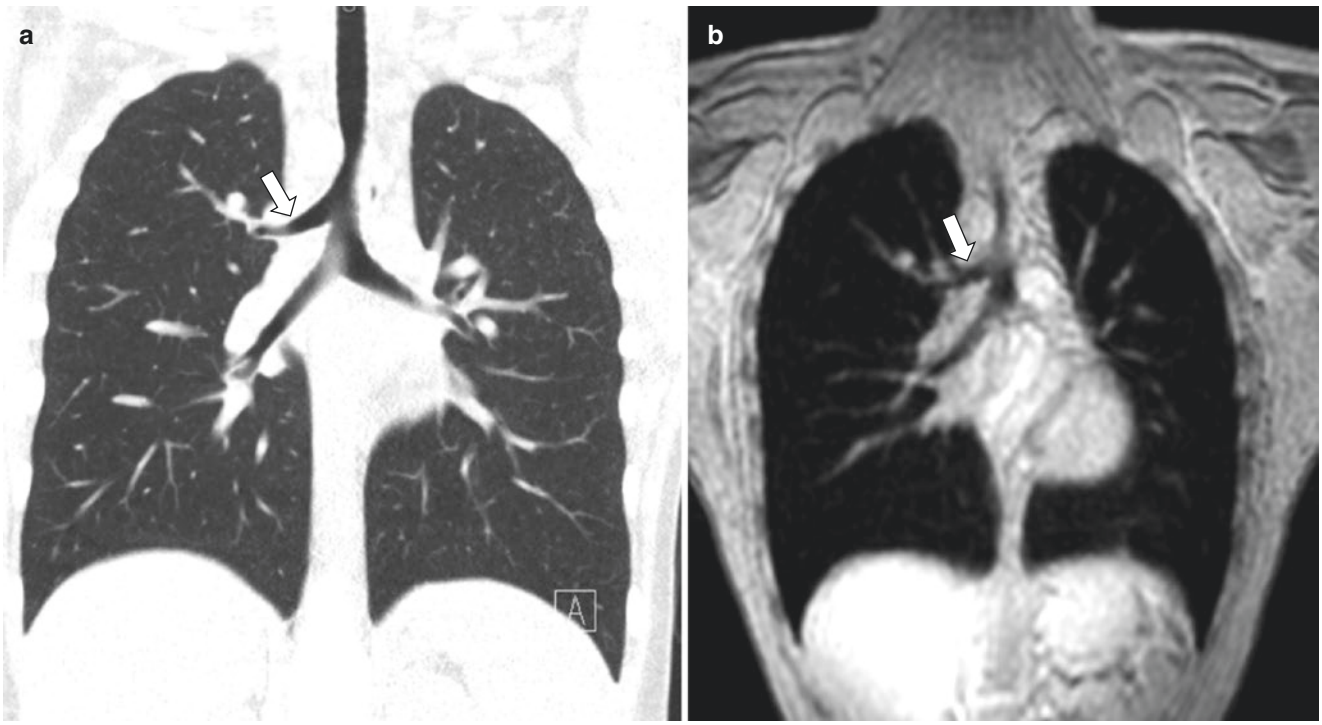

Fig. 2.21 Tracheal bronchus in a 16-year-old boy. (**a**) Coronal enhanced lung window setting CT image shows the right upper lobe bronchus (*arrow*) arising directly from the trachea. (**b**) Coronal enhanced T2-weighted HASTE MR image shows the right upper lobe bronchus (*arrow*) arising directly from the trachea

originating directly from the trachea [17]. Breath-hold acquisition at end-inspiration acquired in the coronal view enhances detection of this aberrant bronchus (Fig. 2.21).

Treatment of TB is based on the severity of the symptoms. Pediatric patients with TB and recurrent respiratory infections are treated with TB resection and lobectomy of the anomalous lobe. If the patient is asymptomatic, expectant management with bronchodilators is preferred [57].

Bronchial Atresia

Bronchial atresia is characterized by focal occlusion of a proximal segmental bronchus, with normal anatomy of the distal bronchial tree [20, 23]. The cause of bronchial atresia is still unclear, although some authors speculate that a vascular interruption during gestation may be the cause [58]. The lung parenchyma distal to the obstruction becomes isolated from the bronchial tree, but it receives collateral ventilation through the pores of Kohn, which are microscopic connections through the walls of adjacent alveoli. The atretic bronchus tends to accumulate mucus, appearing as a closed tubular structure filled with fluid and known as bronchocele [55]. Bronchial atresia is more frequently seen in the upper lobes, most often the apical-posterior segment of the left upper lobe [59]. Bronchial atresia is usually asymptomatic, although mild dyspnea, cough, and repeated infection may occur in approximately 30% of the cases [60].

On CT, bronchial atresia appears as centrally located tubular-shaped structure radiating from the airways associated with mucus impaction and hyperlucent lung parenchyma. On MR imaging, bronchial atresia is well depicted with T2-weighted sequences, showing hyperintense signal intensity (SI) in the impacted mucus (Fig.2.22) surrounded by low SI lung parenchyma due to the chronic hyperinflation and oligemia. In order to increase detection of hyperinflation, imaging in the expiratory phase helps provide better contrast against the adjacent normal relatively hyperintense lung tissue [17]. The differential diagnosis of bronchial atresia includes all pathologies that can fill airways with mucus, such as bronchiectasis, allergic bronchopulmonary aspergillosis (ABPA), and tumor obstruction.

When asymptomatic, bronchial atresia is typically treated conservatively. When associated with symptoms, including recurrent infection, surgical resection is typically performed.

Bronchogenic Cyst

Bronchogenic cysts are remnants of the foregut (pulmonary bud), which result from anomalous ramifications arising during the development of the tracheobronchial tree [55, 61]. They have thin walls covered by columnar epithelium producing serous or mucinous material. The position of bronchogenic cysts depends on the embryological period when the defect occurs. If they develop in the early phase, they are typically located in the pericarinal region, and if they develop in a later phase, they are located within the lung parenchyma. Bronchogenic cysts are most frequently located in the subcarinal space, followed by the paratracheal regions and intra-pulmonary locations, especially the lower lobes. Rarely, bronchogenic cysts can be found in the posterior mediastinum or in an infra-diaphragmatic location [61]. Bronchogenic cysts can be asymptomatic and discovered

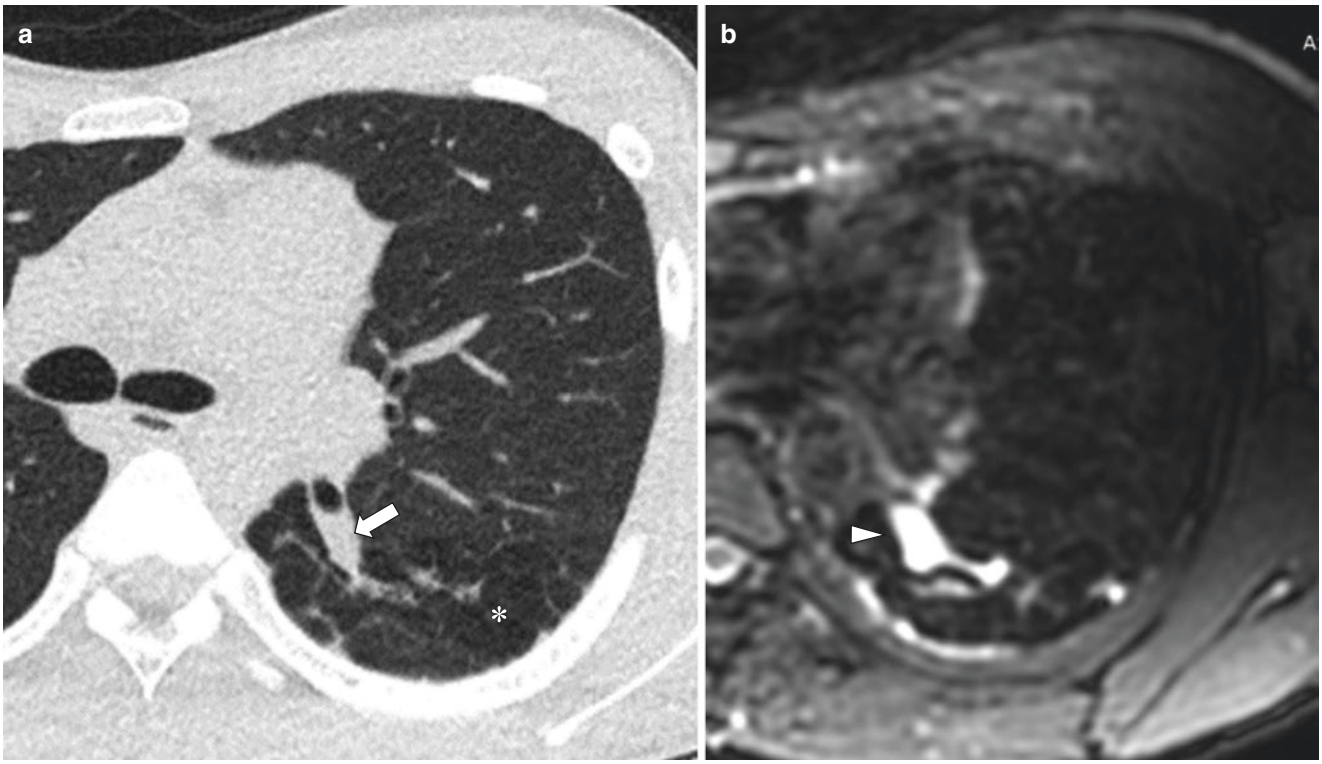

Fig. 2.22 Bronchial atresia in a 17-year-old boy. (**a**) Axial nonenhanced lung window setting CT image shows a tubular fluid-filled structure (*arrow*) in the left upper lobe compatible with bronchial atresia and air trapping (*) within the left upper lobe. (**b**) Axial nonenhanced T2-weighted CUBE (GE) MR image shows hyperintense signal intensity material (*arrowhead*) filling bronchial atresia. Air trapping seen on CT is not as easily seen on MR image

as incidental findings, although they can cause symptoms if superinfection occurs or if they compress surrounding structures, such as the trachea, bronchi, or esophagus.

On CXR, bronchogenic cysts appear as solitary rounded or oval opacities with well-defined contours and uniform density, which can contain an air-fluid level. On CT, they appear as solitary ovoid or rounded lesions with well-defined contours. In 50% of cases, bronchogenic cysts have a density similar to that of water, but they can be denser depending on the contents of the cyst. In cases of superinfection and communication with the airways, they can also contain blood, air, or gas [61]. Atypical features of bronchogenic cysts include thick wall, solid content, calcifications, or septa. MR imaging is an efficient alternative to CT to diagnose bronchogenic cysts. They typically demonstrate hypo- or isointense signal on T1-weighted sequences and hyperintense homogeneous signal on T2-weighted sequences, reflecting presence of water (Fig. 2.23) [17]. On post-contrast MR imaging, bronchogenic cysts show rim enhancement, typical of cystic lesions. Differential diagnosis includes esophageal duplication cyst (in the middle mediastinum) and neurogenic cyst (in the posterior mediastinum). Final diagnosis is confirmed by the presence of respiratory epithelium in the pathology specimen.

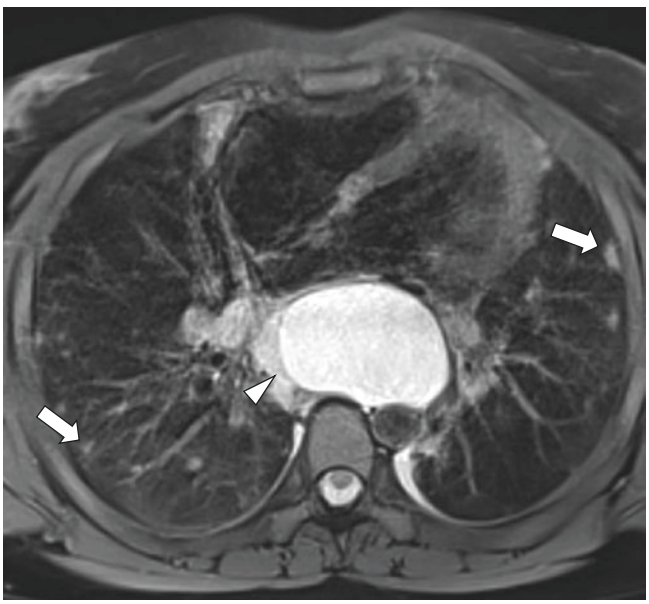

Fig. 2.23 Congenital bronchogenic cyst in a 13-year-old girl with common variable immunodeficiency (CVID). Axial nonenhanced T2-weighted PROPELLER MR image shows a hyperintense cyst (*arrowhead*) in the subcarinal region and multiple subpleural nodules (*arrows*) representing granulomas due to CVID

Typical treatment of bronchogenic cysts is surgical resection, especially when symptomatic. Some authors suggest early surgery in the post-natal period because it provides better conservation of pulmonary parenchyma, a lower incidence of inflammatory lesions, and a reduced rate of complications [62]. However, in asymptomatic patients, surgery is debated because it is associated with 20% morbidity [63, 64]. When conservative management is employed, affected patients should be informed of the 45% of risk of developing symptoms, of a 0.7% risk of developing a malignancy, and that a close long-term follow-up strategy is warranted [63, 64].

Congenital Dynamic Large Airway Disorders

Obstructive Sleep Apnea Syndrome

Obstructive sleep apnea syndrome (OSAS) is a relatively common sleep disorder, in which there is complete or partial upper airway collapse and obstruction during sleep. Typical symptoms include loud snoring or choking, frequent awakenings, disrupted sleep, excessive daytime sleepiness, fatigue, and impaired cognition [65]. Diagnosis is made by measuring the apnea-hypopnea index (AHI). AHI is considered positive for OSAS when there are five or more episodes of apnea and hypopnea per hour of sleep and associated symptoms or when there are 15 or more obstructive apnea-hypopnea events per hour of sleep regardless of symptoms.

OSAS is far more common in adult patients than children where relevant risk factors are obesity, male gender, and increasing age. In contrast, in pediatric OSAS, common risk factors are adeno-tonsillar hypertrophy, obesity, hypotonic neuromuscular diseases, and craniofacial anomalies, with a prevalence of up to 3% in children [66]. Snoring is the most common complaint in children with OSAS. Young children may present with agitated sleep and abnormal sleep positions (i.e., neck hyperextension) due to a disordered breathing. Older children often exhibit excessive daytime sleepiness with hyperactivity or inattention. When untreated, OSAS might result in cognitive deficits, attention deficit/hyperactivity disorder, poor academic achievement, and emotional instability.

Although diagnosis of pediatric OSAS is largely based on clinical history and polysomnography, imaging evaluation can be crucial to determine the cause of upper airway obstruction. Paranasal sinus radiograph and lateral neck radiograph (cephalometric analysis) are simple and highly useful methods for the detection craniofacial deformities, sinusitis, and adenoid hypertrophy [67]. With cephalometric analysis, several measurements can be performed in anatomical sites which can predispose patients to OSAS [67]. Although radiographic cephalometric analysis is often performed, both MR imaging and CT provide the advantage of multiplanar visualization [67]. MR imaging allows a better anatomical resolution of soft tissue and it does not use ionizing radiation; therefore, it has become the major imaging method for this type of investigation [68]. MR imaging protocols for upper airways should include axial and sagittal images of the oropharyngeal and hypopharyngeal regions to assess the airway contour, the maxillomandibular relationship (e.g., retrognathia and micrognathia), the soft palate, the palate shape, the position of the hyoid bone, and the position and volume of the dorsum of the tongue. Axial reconstructions are important to assess the nasopharynx, hypopharynx, palate, dorsum of the tongue, and vocal cords [68]. Cine-MR imaging of the upper airway is particularly helpful in evaluating children with multiple sites of obstruction and to assess both static and dynamic sites of obstruction. MR images are obtained with mild sedation administered by an anesthesiologist. In these examinations, children without OSAS have minimal motion in the airway (less than 5 mm of movement), at the level of the nasopharynx, the posterior oropharynx, and the hypopharynx. However, in children with OSAS, there is typically movement greater than 5 mm at these three levels [69].

Several surgical and non-surgical treatment options for childhood OSAS are currently available, although adenotonsillectomy remains the first line therapy [70–72]. The most used nonsurgical treatment of OSAS is continuous positive airway pressure (CPAP), which is often very effective and well tolerated by many children [74, 75].

Tracheobronchomalacia

Tracheobronchomalacia (TBM) is due to a weakness of the tracheobronchial wall and/or supporting cartilage with consequent excessive collapse of the trachea and bronchi [73]. It may be congenital or secondary to trauma, infection, chronic external compression, or chronic inflammation. TBM is classified based on the etiology [74]. Type 1 lacks external compression and corresponds to "primary tracheomalacia." Type 2 is characterized by extrinsic tracheal and/or bronchial compression, which originates mainly from cardiovascular anomalies, tumors, cysts, or deformities of the chest wall (either congenital or acquired). Type 3 is an acquired malacia arising from prolonged increased ventilatory airway pressure, tracheostomy, or inflammation.

Although bronchoscopy is considered the gold standard to reach diagnosis, imaging shows similar or higher sensitivity compared to bronchoscopy [75]. End-inspiratory and end/forced -expiratory CT imaging is the most used technique to diagnose TBM, and a 50% expiratory reduction in the cross-sectional luminal area is the most often cited criteria for diagnosis of TBM in children [4]. However, this threshold might be too low, as studies in healthy adult subjects have shown that a higher threshold of 70% may be more appropriate to make the diagnosis of TBM [76]. Both bronchoscopy and CT have disadvantages when used in the pediatric population. Bronchoscopy is an invasive procedure that requires anesthesia and CT exposes children to

ionizing radiation. In contrast, MR imaging can be performed in free-breathing conditions in infants with no need for anesthesia, or in older children during forced expiration to elicit better the point of airway collapse [18]. Static and dynamic MR imaging are able to demonstrate airway collapse with the same accuracy of CT without the need for ionizing radiation [19] (Fig. 2.24).

TBM is often self-limited and tends to resolve or become asymptomatic as children grow older [77, 78]. Treatment of symptomatic children with TBM includes bronchodilators, nebulized hypertonic saline to improve mucus clearance, and low-dose inhaled steroids to reduce mucosal swelling and inflammation. CPAP is also often an effective non-surgical treatment for TBM. Surgical treatment in TBM includes aortopexy, slide tracheoplasty, and stent or external splint placement [77, 78].

Infectious and Inflammatory Large Airway Disorders

Tuberculosis

Tuberculosis (TB) remains an important health issue, especially in undeveloped countries. According to the WHO, there were 234,000 deaths due to TB in children <15 years in 2018. In developed countries, TB is rare with an incidence of approximately 4% both in the United States [79] and Europe [80]. Although the primary site of infection is the lung, extrapulmonary TB can occur in children in other organs, mostly lymph nodes and the central nervous system. Typical symptoms of pulmonary TB include cough, fever, night sweats, and weight loss.

Initial screening for TB infection is usually obtained with tuberculin skin test (TST), followed by imaging. Imaging evaluation is particularly important in infants and young children, who may be asymptomatic but with a positive TST. CXR is the most frequently used screening study for TB infection because of its low cost and high availability. A common finding on CXR in a child with TB is a primary complex, which consists of a focal parenchymal opacity with hilar or subcarinal lymphadenopathy [81–83]. When disease progresses, the compression of large airways due to adenopathy often leads to development of pulmonary consolidation or atelectasis. In older pediatric patients, imaging findings of TB that are more typically seen in adults are often present on CXR, such as upper lobe airspace disease, cavitation, and pleural effusions. CT allows for better assessment of endobronchial involvement, bronchiectasis, and cavitation from TB infection [83].

The routine use of CT in TB patients is debated especially due to concern about ionizing radiation [83]. For this reason, MR imaging has been proposed as possible alternative for follow-up imaging [84]. Compared with CT, MR imaging shows similar accuracy for identifying lung lesions in non-AIDS patients with non-miliary pulmonary tuberculosis and has been shown to have a higher diagnostic performance for detecting pulmonary tissue abnormalities, mediastinal nodes, pleural abnormalities, and presence of caseation resolution [84, 85]. A combination of diffusion-weighted imaging (DWI) and subtracted contrast-enhanced (CE) MR imaging is helpful to assess disease activity in cases of mediastinal nodes/fibrosis (Fig. 2.25) [17]. Presence of diffusion restriction in the lymph nodes and peripheral enhancement suggest active TB.

Different multi-antibiotic therapy regimens are used to treat TB, such as 6–9 months of daily isoniazid, shorter two-drug regime of once-weekly isoniazid and rifapentine, or 4 months of daily rifampin [86]. Selection of the regimen depends on patient's antibiotic tolerance and treatment's adherence.

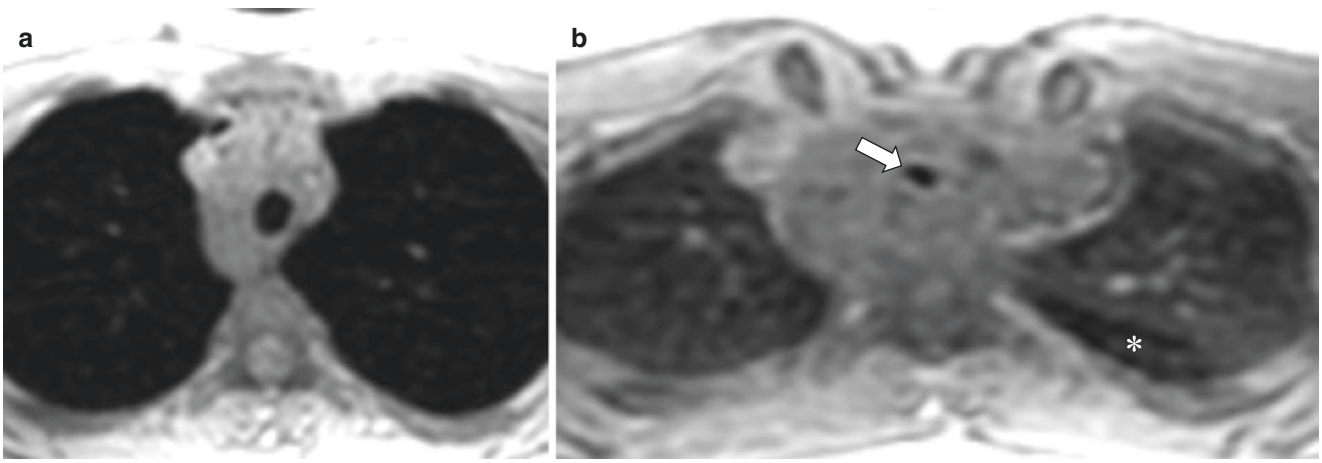

Fig. 2.24 Tracheomalacia in a 17-year-old boy with history of tracheoesophageal fistula. (**a**) Axial nonenhanced proton density-weighted 3D SPGR MR image obtained at end inspiration shows a normal caliber trachea. (**b**) Axial nonenhanced proton density-weighted 3D SPGR MR image obtained at end expiration shows 75% collapse of the trachea (*arrow*) and air trapping (*asterisk*) in the left lower lobe

Histoplasmosis

Histoplasmosis is a fungal infection caused by *Histoplasma capsulatum* frequently found worldwide but especially in North and Central America. In the United States, it is most commonly seen in the state of Ohio and the region of the Mississippi River valley [87]. Typical symptoms of pulmonary histoplasmosis include chest pain, chills, cough, fever, muscle aches and stiffness, and rash (usually small sores on the lower legs).

On CXR, pulmonary histoplasmosis can present as pneumonia with pulmonary nodules containing calcification or cavitation and mediastinal or hilar lymphadenopathy (Fig. 2.26). Because the imaging findings of pulmonary histoplasmosis are similar to TB and sarcoidosis, serology is crucial to narrow the differential diagnosis. Associated findings in histoplasmosis infection include formation of histoplasmoma (bull's-eye calcification in center of nodule), broncholithiasis, fibrosing mediastinitis, and multiple punctate splenic calcifications. Although CXR and chest CT remain the most used techniques to assess pulmonary histoplasmosis, MR imaging has been described as alternative imaging modality to assess mediastinal lymphadenopathy and response to treatment [88].

A rare complication of histoplasmosis infection is fibrosing mediastinitis (FM) [89]. FM is the deposition of collagen and fibrous tissue within the mediastinum caused by an abnormal immunologic response to histoplasmosis infection. FM is more frequently seen in young patients and it can cause compression of the superior vena cava, pulmonary veins/arteries, large airways, or esophagus. FM can be focal or diffuse.

The focal type typically appears on CT and MR imaging as localized, calcified mass in the paratracheal/subcarinal

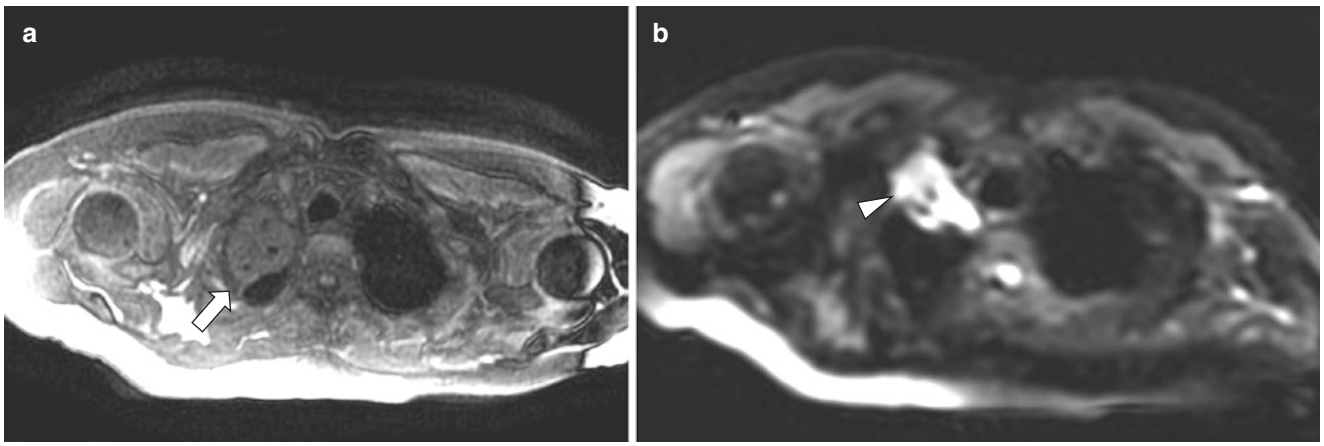

Fig. 2.25 Tuberculosis in a 16-year-old boy who presented with cough, low-grade fever, and weight loss. (Case courtesy of Vincenzo Schininà, Department of Radiology, "L. Spallanzani" National Institute for Infectious Diseases (INMI), IRCCS, Rome, Italy). (**a**) Axial nonenhanced T1-weighted SPGR MR image shows right upper lobe consolidation (*arrow*). (**b**) Axial nonenhanced diffusion weighted MR image (b = 600 s/mm^2) shows restricted diffusion (*arrowhead*) within the region of consolidation

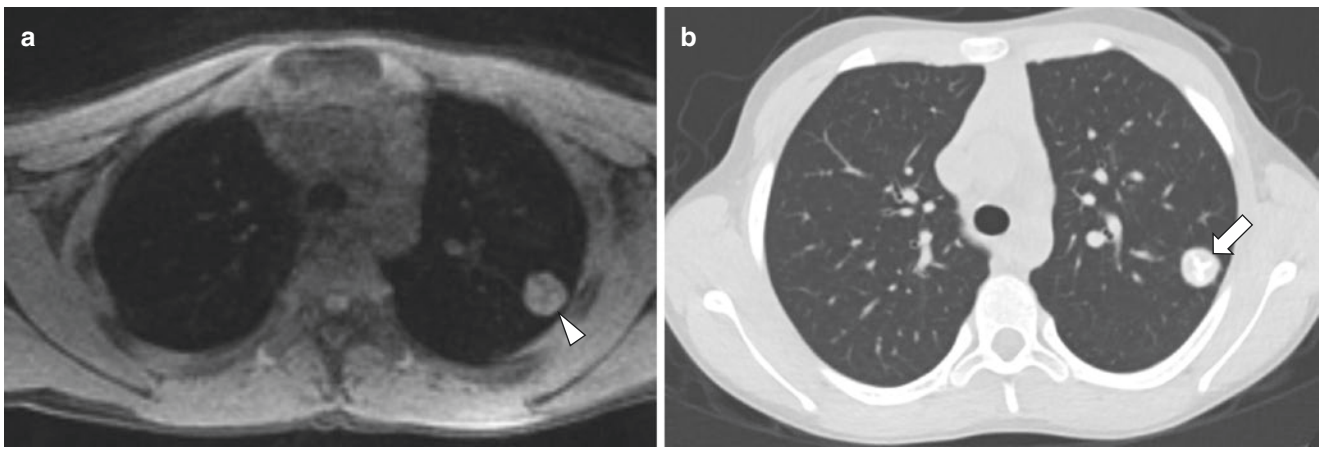

Fig. 2.26 Histoplasmosis infection in a 9-year-old boy. (**a**) Axial nonenhanced proton density-weighted LAVA MR image with fat suppression shows left upper lobe nodule (*arrowhead*) containing propeller-shaped linear regions of central hypointensity. (**b**) Axial nonenhanced lung window setting CT image shows the left upper lobe nodule (*arrow*), and propeller-shaped linear region is hyperdense compatible with calcification

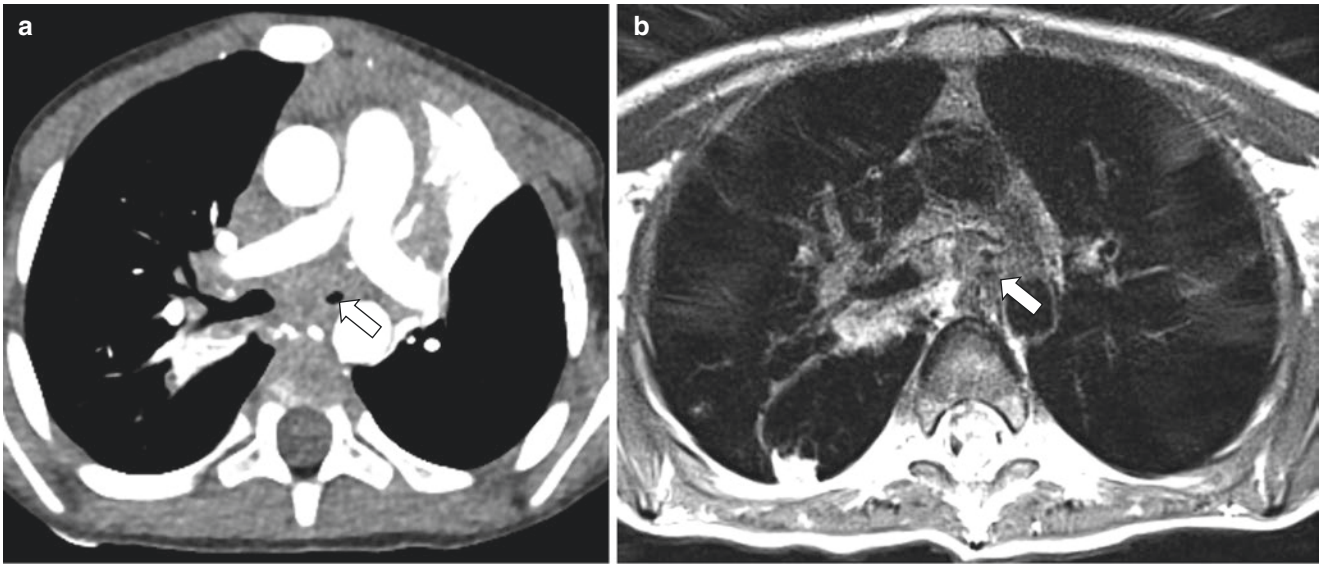

Fig. 2.27 Fibrosing mediastinitis in a 4-year-old boy who presented with progressively worsening shortness of breath and chest pain. (**a**) Axial enhanced soft tissue window setting CT image shows excessive soft tissue in the mediastinum and around the large airways with compression of the left main bronchus (*arrow*). (**b**) Axial nonenhanced T2-weighted PROPELLER MR image also shows the excessive soft tissue in the mediastinum and around the large airways with compression of the left main bronchus (*arrow*)

regions of the mediastinum or in the pulmonary hila. The diffuse type typically appears as an infiltrating mass in multiple mediastinal compartments. Contrast-enhanced imaging is useful to assess the extent, level, and length of stenosis of the mediastinal vessels and large airways. On MR imaging, FM typically appears as a heterogeneous, infiltrative mass of intermediate signal intensity on T1-weighted images and mixed areas of hypo- and hyperintensity on T2-weighted images due to areas of calcification and fibrous tissue (low SI) and areas of active inflammation (high SI) [89] (Fig. 2.27). Heterogeneous enhancement of the mass is typically seen after administration of contrast.

Treatment of pulmonary histoplasmosis includes amphotericin B for 2 weeks followed by itraconazole for a total of 10 weeks. Corticosteroids are given along with the antifungal therapy in those with severe respiratory symptoms [90]. Antifungal therapy is not typically utilized in FM. In severe cases, stents may be placed within the airways and vessels to prevent compression, and surgery may be utilized in cases of refractory disease [90].

Neoplastic Large Airway Disorders

Benign Primary Large Airway Neoplasms

Subglottic Hemangioma Infantile hemangioma is the most common pediatric tumor of head and neck [91]. It consists of a proliferation of capillaries and usually presents within the first month of life. When located in the subglottic region, infantile hemangioma can be associated with upper airway obstruction. Affected pediatric patients typically have biphasic stridor due to upper airway narrowing. Infantile hemangioma has an initial proliferative phase with rapid growth in the first year. They tend to then grow at a slower rate until age of 5 years followed by an involution phase that occurs at 5–7 years.

Because hemangiomas have a typical appearance on visual inspection, imaging may not be necessary, although it is often employed when complications are suspected or to determine the relationship with adjacent airways and mediastinal vessels. Initial screening is typically performed with ultrasound, typically showing a lobulated echogenic mass containing high-flow arteries and veins. On contrast-enhanced CT, infantile hemangiomas show characteristic homogeneous enhancement and rapid wash-out. On MR imaging, the appearance is usually slightly hypointense to muscle on T1-weighted images and iso- to hyperintense on T2-weighted images with flow voids and avid contrast enhancement (Fig. 2.28). In the involution phase, hemangiomas are characterized by accumulation of fibro-fatty tissue, replacing the vascular tissue [92].

Because nearly all infantile hemangiomas eventually involute, a conservative wait-and-see approach is used for those minimally symptomatic or asymptomatic pediatric patients [93]. Symptomatic patients are often initially treated with medications that accelerate involution of the infantile hemangioma, such as propanolol. Second-line pharmacotherapy includes corticosteroids, which are used in refractory cases. Surgical options may include intralesional injection with corticosteroids, ablation, or surgical excision [93].

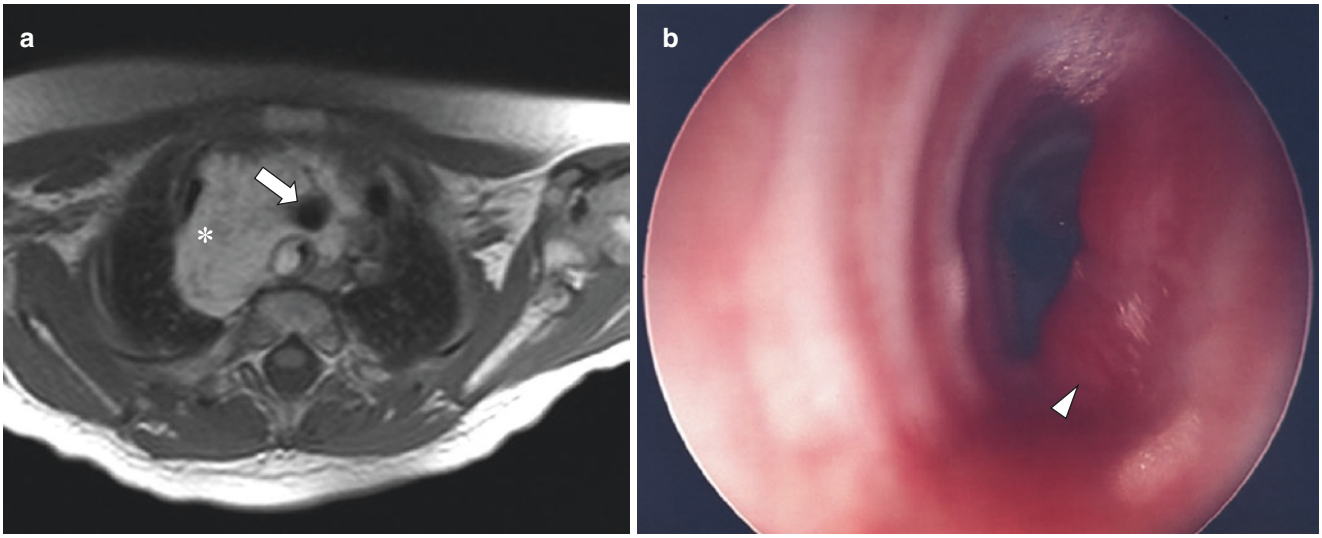

Fig. 2.28 Large airway hemangioma in a 3-month-old girl who presented with respiratory distress and subcutaneous hemangiomas. (**a**) Axial T1-weighted GRE MR image shows hyperintense lesion (*asterisk*) of the mediastinum with encasement and compression of the trachea (*arrow*). (**b**) Endoscopy image shows typical appearance of this hypervascular lesion (*arrowhead*), extending into the trachea lumen with narrowing

Respiratory Papillomatosis Respiratory papillomatosis (RP) is a condition characterized by multiple papillomas in the respiratory epithelium [94]. This occurs more commonly in the upper airways at the level of the larynx (laryngeal papillomatosis) than in the central airways (tracheobronchial papillomatosis). RP is the most common benign tumor of the trachea in children (60% of all benign tumors) [94]. RP is caused by human papilloma virus (HPV) infection, especially types 6 and 11. Human papilloma virus also causes skin and genital warts. Airway infection in children is thought to occur due to transmission to the newborn during vaginal delivery. Symptoms of chronic cough, wheezing, stridor, and hemoptysis can be present around age 2–3 years in affected patients.

The current gold standard for diagnosis is bronchoscopy, which allows direct visualization and therapeutic intervention with direct removal of the lesions. On CXR, papillomas are usually not visible, although when involving the lung parenchyma, they may appear as multiple pulmonary nodules, sometimes with cavitation. CT is the preferred method to assess the extent of disease [94]. Typical CT findings include tracheal nodules, solid or cavitated nodules in the lung parenchyma, air trapping, masses, and consolidation [94]. MR imaging can be also used as alternative to CT to visualize both airways and parenchymal changes due to RP while at the same time limiting radiation exposure. On MR imaging, papillomas typically appear as endobronchial lesions protruding into the airway lumen or as multiple lung nodules.

To date, no curative treatment for RP exists, and surgical excision of the papillomas remains the mainstay of therapy [95]. Unfortunately, lesion recurrence after surgery is common and in those patients who undergo multiple procedures, surgical complications such as larynx and glottis stenosis may occur. Coadjuvant medical treatment with agents including interferon, antiviral agents (acyclovir, ribavirin, cidofovir), retinoids, and inhibitors of the oxygenase-2 cycle may be utilized to limit HPV replication and proliferation [95].

Neurofibroma Neurofibromas are associated with neurofibromatosis type 1 (NF1) and can occur throughout the body, including the neck, thorax, and airways. NF1 is an autosomal dominant disorder and is the most common phakomatosis with an incidence 1/2000 live births [96]. In up to 50% of cases, NF1 occurs with no family history due to a sporadic spontaneous mutation.

Neurofibromas can present as a single large lesion (plexiform neurofibroma) or multiple small neurofibromas. Plexiform neurofibromas represent diffuse neural enlargement or multiple neurofibromas along the course of peripheral nerves. In the thorax, neurofibromas may involve the ribs, chest wall, lungs, and mediastinum. Mediastinal neurofibromas can cause compression of the central airway and mediastinal vessels. Furthermore, neurofibromas can directly arise from the trachea and esophagus [97]. Although diagnosis is based on clinical and genetic testing, imaging is important to assess the extension of the lesions, effect on surrounding structures and treatment planning.

On CT, neurofibromas typically have a central region of low attenuation, seen in two-thirds of the cases [96]. Sometimes, the central region of hypoattenuation tends to enhance giving a typical "target" sign appearance. On MR imaging, neurofibromas often demonstrate peripheral hyperintensity surrounding a region of central hypointensity on T2-weighted images, and enhancement may be heterogeneous if large [98] (Fig. 2.29). Plexiform neurofibromas are a more extensive form of neurofibroma that are infiltrative and have rope-like extensions along the course of the nerve with variable enhancement [98].

Asymptomatic neurofibromas are typically managed conservatively. Symptomatic mediastinal neurofibromas are usually surgically resected to decompress affected mediastinal structures [99].

Malignant Primary Large Airway Neoplasms

Tumors of the Tongue In the pediatric population, tumors of the oral cavity are more frequently benign with malignant tumors representing only 10% of oral cavity tumors. Malignant tumors include (in order of frequency) rhabdomyosarcoma, fibrosarcoma, carcinoma of the parotid, osteosarcoma, and metastatic disease [100, 101]. Among malignant tumors, rhabdomyosarcomas (RMS) are the most common. RMS is a malignant soft tissue tumor that originates from immature striated skeletal muscle cells. RMS of the head and neck region have a low tendency to cause lymph node involvement [100], but distant metastasis to other organs may occur.

Both CT and MR imaging can be used to assess the primary site of the tumor and the relationship with the surrounding structures [37]. However, MR imaging is increasingly preferred as the primary imaging method, especially for head and neck localization, because of its multiplanar capacity, ability to attenuate bone artifact, and superior soft tissue contrast. Findings on CT and MR imaging typically show an inhomogeneous solid mass with avid enhancement and variable obstruction of the oral airway (Fig. 2.30). Intratumoral necrosis, hemorrhage and adjacent bone destruction are often present. Disease staging for metastasis uses CT and/or radionuclide scans such as PET [37].

Treatment of RMS is based on a multimodal approach including surgery, chemotherapy, and/or radiation [102]. Treatment-associated sequelae may be impaired growth and function of the maxilla associated with local radiation therapy and scarring.

Nasopharyngeal Tumor Nasopharyngeal tumors are rare in children representing only 1% of malignancies in childhood [103–105]. These tumors are more frequent in Asian and Northern African children and are strongly associated with Epstein-Barr-virus infection. Peak incidence is between ages 10 and 19 years. Typical symptoms include nasal obstruction and discharge, epistaxis, hearing impairment, and neck swelling due to lymphadenopathy. Cranial

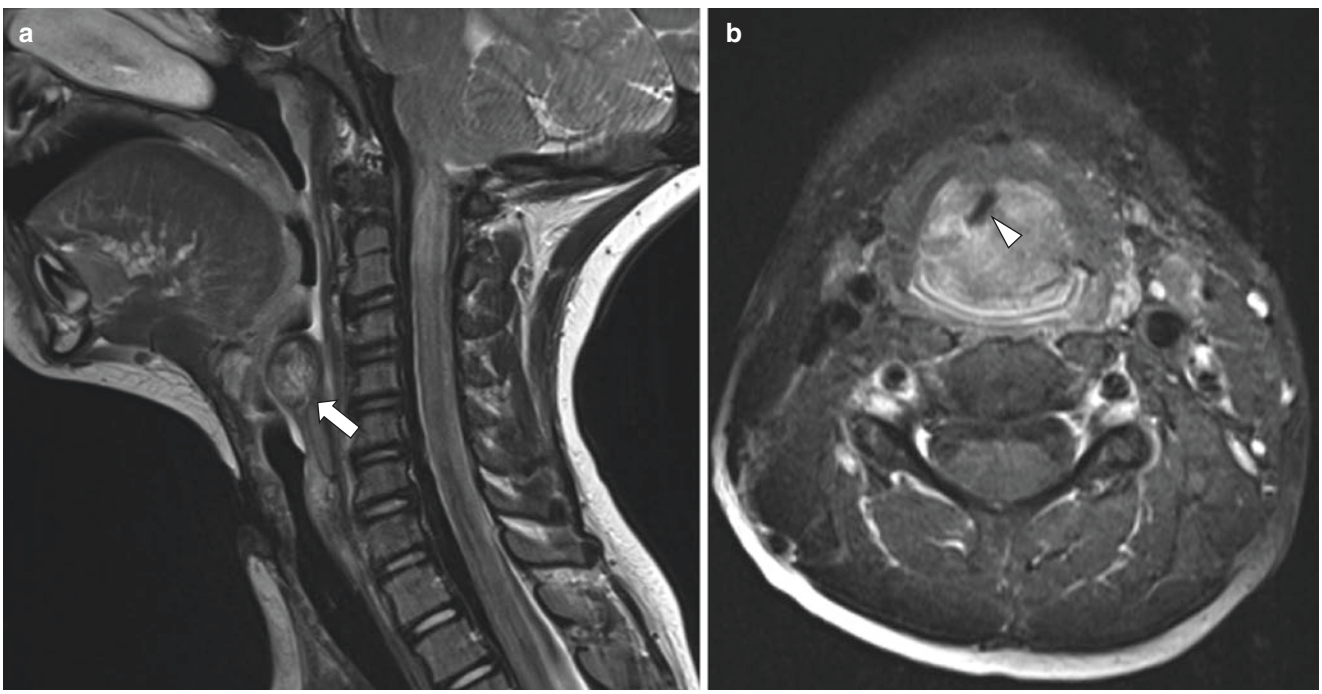

Fig. 2.29 Airway neurofibroma in a 6-year-old girl who presented with stridor. (**a**) Sagittal nonenhanced T1-weighted GRE MR image shows a nodular lesion (*arrow*) in the hypopharynx. (**b**) Axial nonenhanced T2-weighted HASTE MR image with fat suppression shows compression of airway (*arrowhead*) at the level of the larynx

nerve palsy may be seen in advanced cases due to skull base infiltration.

On CT and MR imaging, nasopharyngeal tumors appear as large inhomogeneous masses expanding into the nasopharyngeal airway, with bone erosion and intracranial extension [105] (Fig. 2.31). The tumor usually arises in the posterolateral wall of the nasopharynx in the fossa of Rosenmüller.

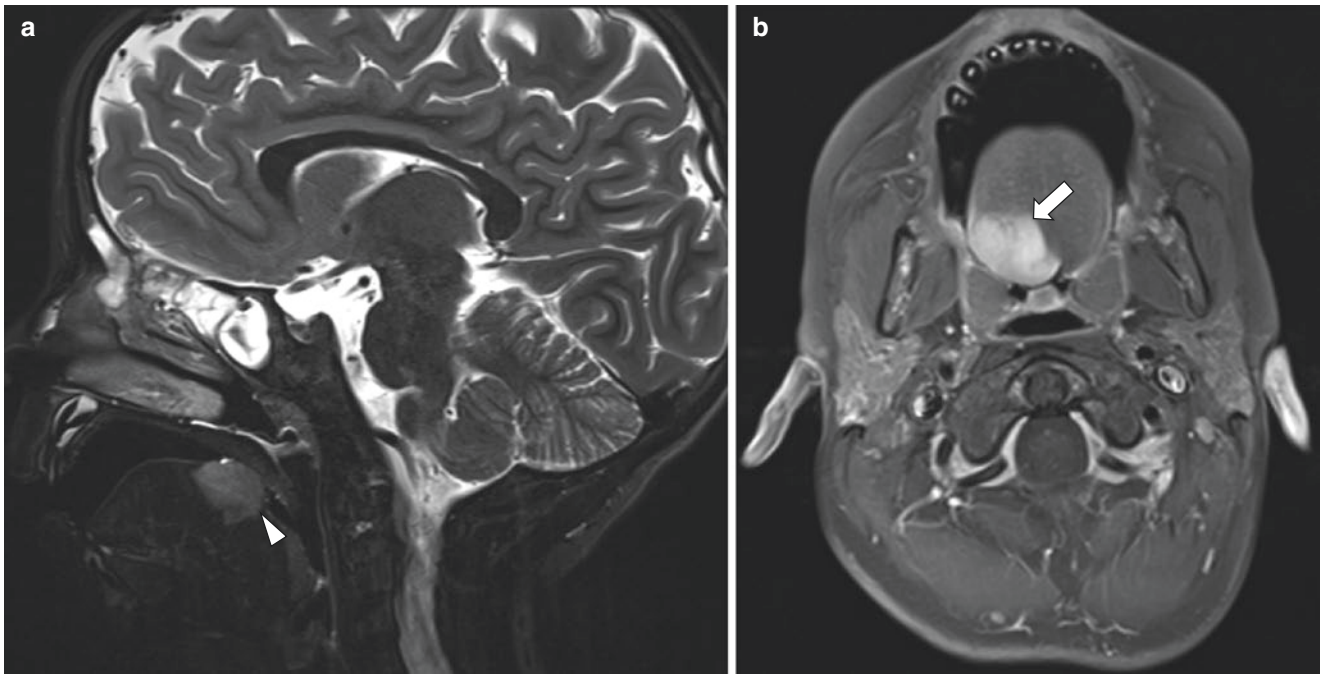

Fig. 2.30 Rhabdomyosarcoma of the tongue in a 4-year-old boy who presented with swallowing difficulty and respiratory distress. (**a**) Sagittal nonenhanced T2-weighted FSE MR image shows a hyperintense mass (*arrowhead*) arising from the right base of the tongue. (**b**) Axial enhanced T1-weighted GRE MR image with fat suppression shows avid enhancement of the mass (*arrow*)

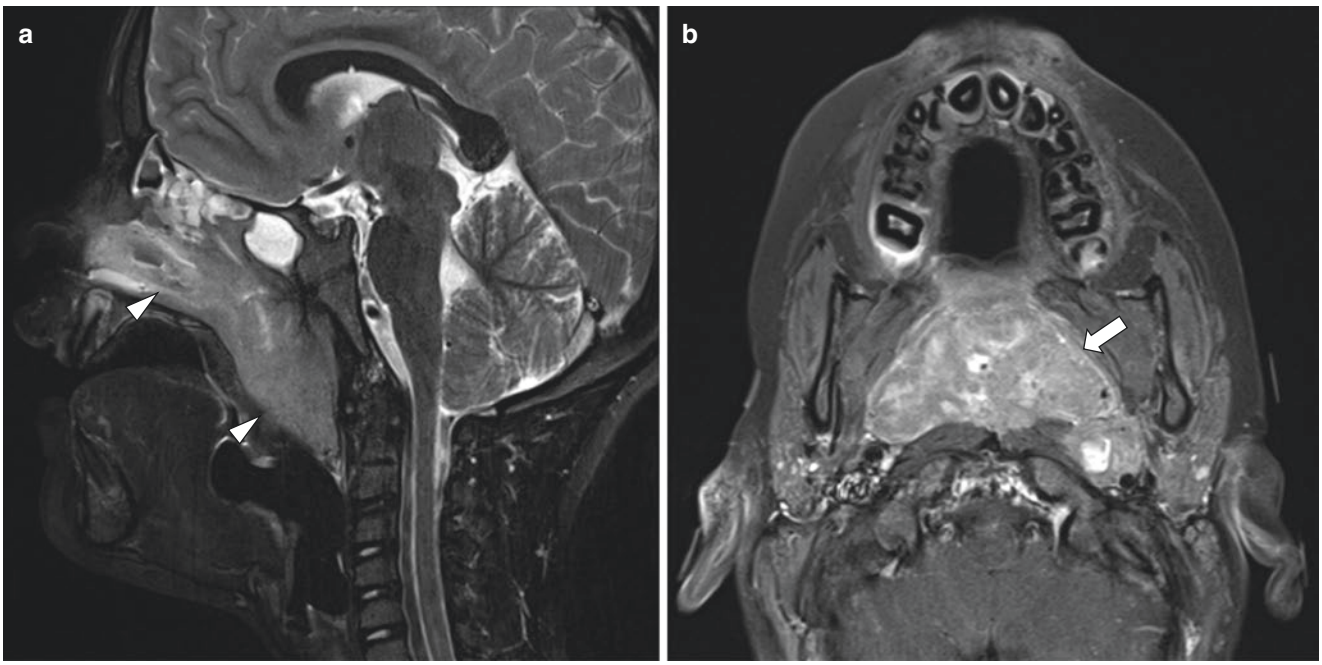

Fig. 2.31 Nasopharyngeal tumor in a 9-year-old girl who presented with respiratory distress and headaches. (**a**) Sagittal nonenhanced T2-weighted spin-echo MR image shows a mass (*arrowheads*) within the nasal cavity and nasopharynx downwardly displacing the soft palate. (**b**) Axial T1-weighted GRE MR image with fat suppression shows airway obstruction by the mass (*arrow*)

The current treatment of nasopharyngeal tumor includes surgery and/or radiation therapy and chemotherapy.

Carcinoid Tumor Although airway carcinoid tumor is rare in children, pulmonary carcinoid is the most common primary lung neoplasm in the pediatric population, typically presenting in late adolescence [106, 107]. Airway carcinoid tumors are frequently located in a main bronchus or in the proximal portion of a lobar bronchus. According to the size and location of the lesion, affected pediatric patients may present with chronic cough, hemoptysis, dyspnea, and persistent partial or total lung atelectasis. Unresolved atelectasis and pneumonia despite antibiotic treatment should suggest a possible airway carcinoid tumor. Other symptoms are related to the production of hormones such as serotonin and other bioactive amines giving cutaneous flushing, diarrhea, and bronchospasm or adrenocorticotropic hormone (ACTH) giving Cushing syndrome [108].

On CXR, carcinoid tumor typically appears as round nodule or mass in a hilar or perihilar location. When causing airway obstruction, atelectasis and mucoid impaction may be visible. Alternatively, airway carcinoid tumors may lead to hyperinflation of the affected lobe by causing a check-valve effect. If airway carcinoid tumor is small and there is no airway obstruction, CXR may be normal. CT is more sensitive than CXR for detection of airway lesions and is able to better visualize extension within and outside the large airways. On CT, carcinoid tumors typically have a lobulated contour with punctate or eccentric calcification [109]. Contrast-enhanced CT frequently shows marked enhancement due to the vascular nature of the tumors. Diagnosis is usually confirmed either by bronchoscopic biopsy (for central lesions) or by transthoracic needle biopsy (for peripheral lesions).

The use of MR imaging to assess carcinoid has been proposed, because of MR imaging's superior ability to characterize different soft tissues [109]. Using in- and out-of-phase techniques, MR imaging can provide information about the tumor fat content, which is often seen in carcinoid [110]. Moreover, MR imaging can be used as a problem-solving tool to clarify equivocal or indeterminate findings on CT. Airway carcinoid tumors show high signal intensity on T2-weighted and short-inversion-time inversion-recovery MR images, which help to distinguish them from adjacent pulmonary vessels, especially in the perihilar regions [110].

The most effective treatment for airway carcinoid tumor is complete surgical excision of the primary tumor. Surgery aims to remove the primary tumor and the involved lymph nodes [107].

Mucoepidermoid Tumor Mucoepidermoid carcinoma (MEC) is the most common malignancy of the salivary gland, accounting for about 3–15% of all salivary gland tumors [103]. Small amounts of salivary gland tissue are present in the submucosa of the trachea. Therefore, MEC can present as airway tumor [107]. Typical symptoms of airway MEC include chronic cough, dyspnea, and hemoptysis. MEC occurs more frequently in segmental bronchi than in the trachea or main bronchi and appear as sharply marginated ovoid or lobulated intraluminal nodules that adapt to the branching features of the airways [107]. MECs tend to have an indolent course characterized by local tumor invasion without metastatic disease.

Although CT is the preferred method to assess local invasion, MR imaging can be considered as alternative to limit radiation exposure in young patients. MECs are typically hypervascular tumors, which may calcify, but do not typically spread to adjacent lymph nodes. Imaging is crucial for surgical and radiation planning to achieve complete surgical resection and avoid local recurrence [111].

Long-term survival rates are excellent when complete surgical resection of MEC is achieved.

Inflammatory Myofibroblastic Tumor Inflammatory myofibroblastic tumors (IMTs) are rare entities and occur predominantly in the lung. Airway IMT is even more rare with a frequency of 0.04–0.07% of all respiratory tract tumors [112]. Initially considered as benign lesion, IMTs tend to show high recurrence rate after resection and occasionally metastasize. Cytogenetic studies have shown that approximately half of IMTs are positive for anaplastic lymphoma kinase gene rearrangements, giving them characteristics of malignant tumors [113]. IMTs consist of myofibroblastic cells and an inflammatory infiltrate of plasma cells, lymphocytes, and eosinophils. When arising in the airway, affected pediatric patients typically present with symptoms of airway obstruction and chronic cough frequently misdiagnosed as asthma or foreign body aspiration in younger children.

Imaging is important to define location and extension of the lesion. Airway IMTs may occur in the trachea or bronchi and when occurring in the trachea often demonstrate full thickness involvement of the membranous wall and the cartilaginous rings. Pulmonary IMTs present as lobulated masses with sharp distinct margins and heterogeneous contrast enhancement (Fig. 2.32). These tumors have a propensity to invade local structures, including vertebrae and thoracic vessels.

Open surgery with complete resection of IMTs is the method of choice to avoid local recurrence. When complete resection is not possible, surgery is combined with radiation therapy and/or chemotherapy.

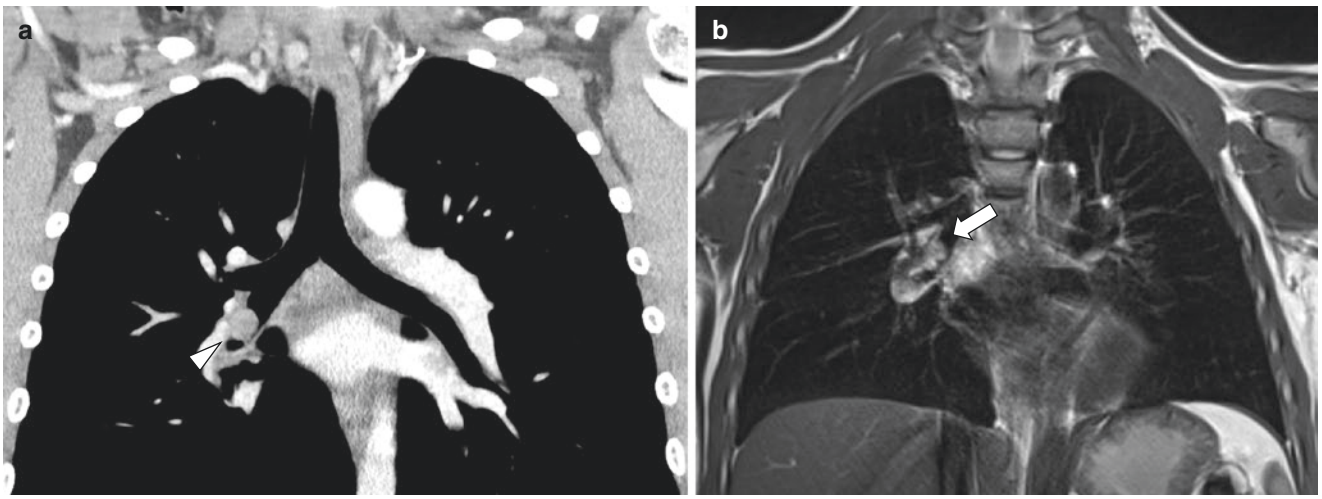

Fig. 2.32 Inflammatory myofibroblastic tumor of the airway in a 9-year-old boy who presented with respiratory distress and right-sided chest pain. (**a**) Coronal enhanced soft tissue window setting CT image shows endobronchial mass (*arrowhead*) within the bronchus intermedius. (**b**) Coronal nonenhanced T2/T1-weighted TrueFISP MR image shows the hyperintense endobronchial mass (*arrow*) within the bronchus intermedius

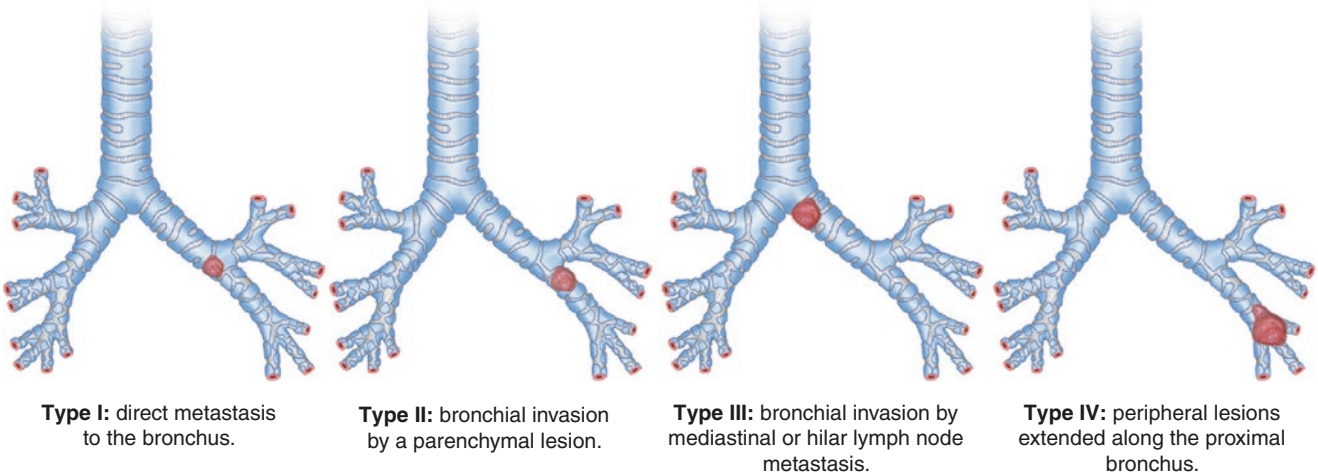

Fig. 2.33 Four modes of endobronchial metastases. (Adapted from Kiryu et al. [116], with permission). Type I: direct metastasis to the bronchus, Type II: bronchial invasion by a parenchymal lesion, Type III: bronchial invasion by mediastinal or hilar lymph node metastasis, Type IV: peripheral lesions extended along the proximal bronchus

Metastatic Large Airway Neoplasms

Large airway metastases can occur from hematogenous tumor seeding in the airways (Type I), from large airway invasion by a nearby parenchymal lesion (Type II), from large airway invasion by mediastinal or hilar lymph node metastasis (Type III), and as peripheral lesions extended along the proximal large airway (Type IV) [114–116] (Fig. 2.33). Hematogenous spread from distant neoplasms directly to large airways (Type I) is extremely rare in pediatric patients. Airway involvement is more frequently due to invasion from an adjacent primary tumor such as mediastinal lymphoma or metastatic lymphadenopathy (Type II) [116]. Lymphoma tends to cause extrinsic compression of the large airways and eventually obstruction. Metastatic mediastinal lymphadenopathy can occur with several other tumors as well, including Wilms tumor, neuroblastoma, testicular neoplasms, and sarcomas.

Both CT and MR imaging can be used to assess the location of an endobronchial lesion, localizing it to the trachea and main, lobar, segmental, or subsegmental bronchi. CT and MR imaging can define the shape of a lesion within the airway as polypoid, finger-in-glove, or bronchial wall thick-

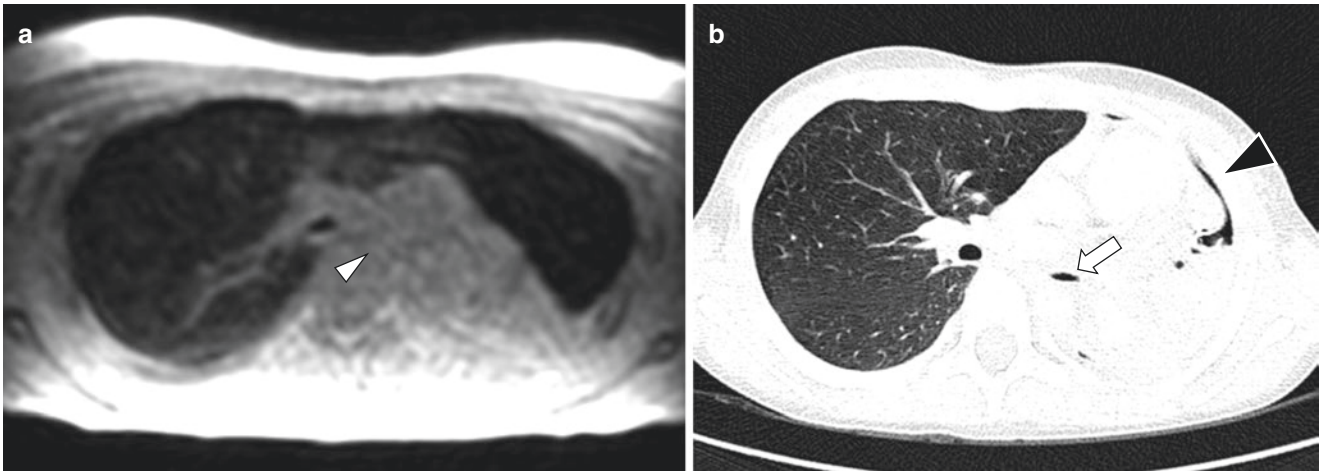

Fig. 2.34 Post-traumatic left main bronchial rupture in a 13-year-old boy who presented with respiratory distress, desaturation, and chest pain. (**a**) Axial reformat of sagittal-acquired nonenhanced proton density-weighted SPGR MR image obtained at end-expiration with nonvisualization of the left main bronchus (*white arrowhead*). (**b**) Axial nonenhanced lung window setting CT image obtained at end-expiration shows compression of the left main bronchus (*arrow*) and pneumomediastinum (*black arrowhead*)

ening. They are also excellent modalities for quantifying the number of lesions [115]. On both CT and MR imaging, metastatic lymph nodes typically appear as nodular conglomerates of enhancing soft tissue, which may develop a hypoenhancing-necrotic center. Large and aggressive tumors may cause extrinsic compression or airway invasion.

According to the type of tumor, location, and extension, a variable combination of chemotherapy and/or radiation therapy and surgery is currently used for treatment of the metastatic neoplasms of the large airways.

Acquired Large Airway Disorders

Acquired Tracheal Stenosis

Acquired tracheal stenosis in children is caused by prolonged endotracheal intubation, tracheostomy tube, or surgery. Injury of the upper airways (larynx and proximal trachea) is most often due to endotracheal intubation in newborns [117]. Infants requiring prolonged positive pressure ventilation via an endotracheal tube for a week or longer and infants requiring repeated intubations are at greatest risk for developing tracheal stenosis. Epithelial damage frequently occurs after endotracheal intubation and is accentuated when tube size does not fit patient's airway size [117]. Post-extubation stridor is the most common sign of moderate to severe subglottic stenosis or laryngeal injury.

Post-traumatic Tracheobronchial Injury

Post-traumatic tracheobronchial injuries are associated with high-energy trauma and have high associated mortality rates. Airway injury is associated with rapid symptoms of dyspnea, subcutaneous emphysema, and stridor [118]. Signs of airway injury on CXR include subcutaneous emphysema and pneumothorax [118]. CT and MR imaging are helpful for confirming the site of airway injury and identifying associated injuries (Fig. 2.34). Treatment of tracheobronchial injuries is surgical, consisting of large airway reconstruction and anastomosis or resection depending on the site of injury and extent of injury.

Postsurgical Bronchial Stenosis

Surgical treatment can also cause airway stenosis, mostly due to postsurgical complications leading to chronic inflammation and fibrosis [115]. On CT or MR imaging, bronchial stenosis appears as a focal narrowing of the airway lumen with eccentric or concentric soft tissue thickening. Causes include pressure necrosis, ischemia, and fibrosis due to the instrumentation during surgery or perianastomotic stenosis in cases of lung transplantation (Fig. 2.35). Most cases can be managed with endoscopic balloon dilation or laser treatment. However, in the most severe cases, open surgery is required.

Foreign Body Aspiration

Foreign body aspiration (FBA) is a common cause of mortality and morbidity in young children [119]. FBA occurs more frequently in the first years of life, when children tend to explore the world by putting objects into their mouths. The majority of aspirated FBs in children are found within the bronchi, especially on the right side, because of the more vertical angulation of the right main bronchus. The typical triad of symptoms in FBA is an episode of choking with severe respiratory distress and cyanosis.

On CXR, characteristic findings in FBA are unilateral hyperinflation and mediastinal shift [120]. Although affected

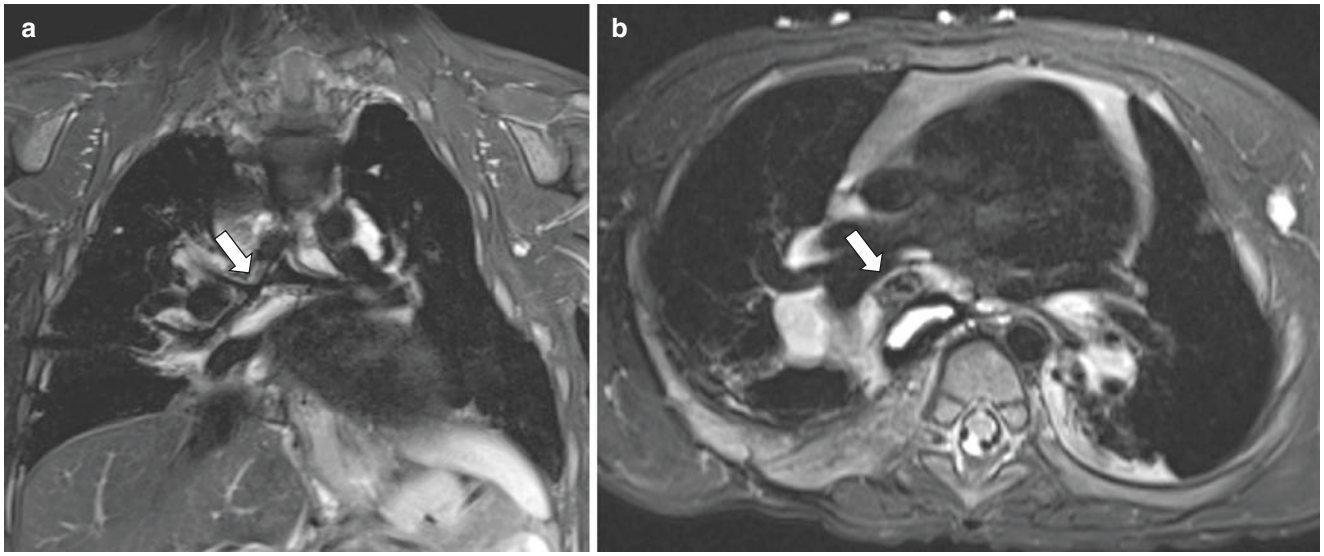

Fig. 2.35 Postsurgical bronchial stenosis in a 3-year-old boy with tracheoesophageal fistula repair. (**a**) Coronal nonenhanced T2-weighted BLADE MR image shows stenosis (*arrow*) of right main bronchus. (**b**) Axial nonenhanced T2-weighted BLADE MR image shows stenosis (*arrow*) of right main bronchus

patients can be further investigated with bronchoscopy after CXR, cross-sectional imaging may be considered in stable pediatric patients with signs and symptoms suspicious for FBA. Findings of FBA on CT and MR imaging may include direct visualization of the foreign body, hyperinflation of a lung or lobe of the lung, and atelectasis of a lung or lobe of the lung [120] (Fig. 2.36).

Bronchoscopy is the gold-standard test for the assessment of FBA, because it allows direct visualization and removal of the FB.

Miscellaneous Large Airway Disorders

Various congenital, inflammatory, or neoplastic masses around the large airways can result in extrinsic compression of the large airway in the pediatric population. Several examples are discussed in the following section.

Lymphatic Malformation

Lymphatic malformations (LMs) are a type of vascular malformation. In general, vascular malformations are classified into low-flow lesions (lymphatic, venous, capillary, or combined) and high-flow lesions (arteriovenous malformations and arteriovenous fistulas) [91, 92, 121].

LMs are the most common low-flow vascular malformations. LMs frequently present as a cystic mass in newborns, although they may also be diagnosed later in life [91, 92, 121]. More than half of LMs are associated with genetic disorders, such as Turner syndrome, Noonan syndrome, and trisomies. LMs are most frequently located in the head and neck region and are the result of an embryological disorder in the development of the cervical lymphatic system. The majority of cervical LMs are diagnosed in newborns and children up to 2 years, with equal distribution between boys and girls. Lesions frequently occur posterior to the sternocleidomastoid muscle, but they can extend around the entire neck and into the mediastinum. On clinical examination, LMs appear as painless slow-growing masses with a spongy

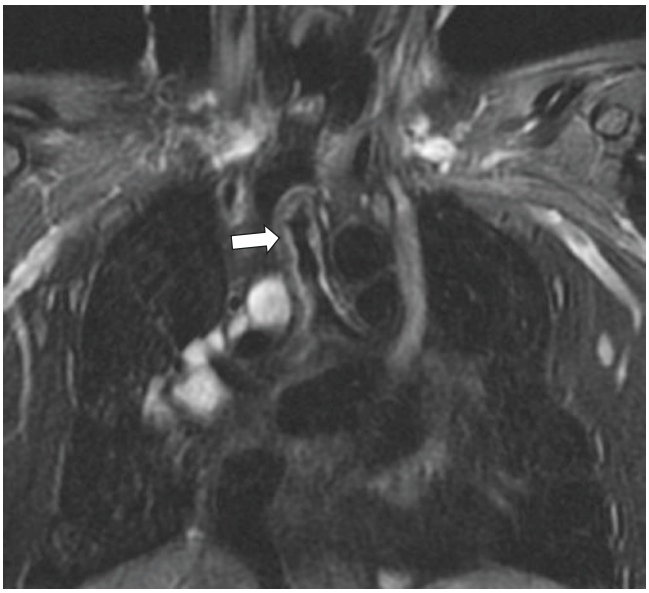

Fig. 2.36 Tracheal changes in a 16-year-old girl with prior history of battery ingestion and erosion into the trachea. Coronal nonenhanced T2-weighted FSE MR image with fat suppression shows long segment irregularity and stenosis of the trachea (*arrow*)

consistency. Infection or hemorrhage can lead to sudden enlargement with increased local compression, including on the airways. LMs are classified as macrocystic (>1 cm), microcystic (<1 cm), and mixed cystic forms [92]. The macrocystic is the most common type.

LMs are typically first assessed with ultrasound, which shows a uni- or multilocular cystic mass, containing fluid. Debris is often seen within the fluid, due to superimposed hemorrhage or infection. Septations of variable thickness are usually seen and may demonstrate color Doppler flow. Microcystic LMs tend to appear predominantly hyperechoic and can be confused with solid soft tissue masses. Cross-sectional imaging with CT and MR imaging are crucial for treatment planning. MR imaging is preferred over CT in order to avoid ionizing radiation exposure and because it better highlights the relationship of the lesion with the surrounding structures.

On MR imaging, LMs typically demonstrate hyperintense signal intensity on T2-weighted images (Fig. 2.37). On T1-weighted images, LMs usually demonstrate low or intermediate signal intensity. Post-contrast imaging shows septal contrast enhancement. In cases of superimposed infection or hemorrhage, the content of the cyst may be hyperintense on T1-weighted images due to the presence of proteinaceous contents and post-contrast imaging may demonstrate increased surrounding enhancement.

Treatment with surgery or intralesional sclerotherapy depends on the extent and relationship with the neighboring structures and to the type of LM. Suprahyoid microcystic LMs are more difficult to treat than macrocystic LMs in the infrahyoid and posterior cervical regions.

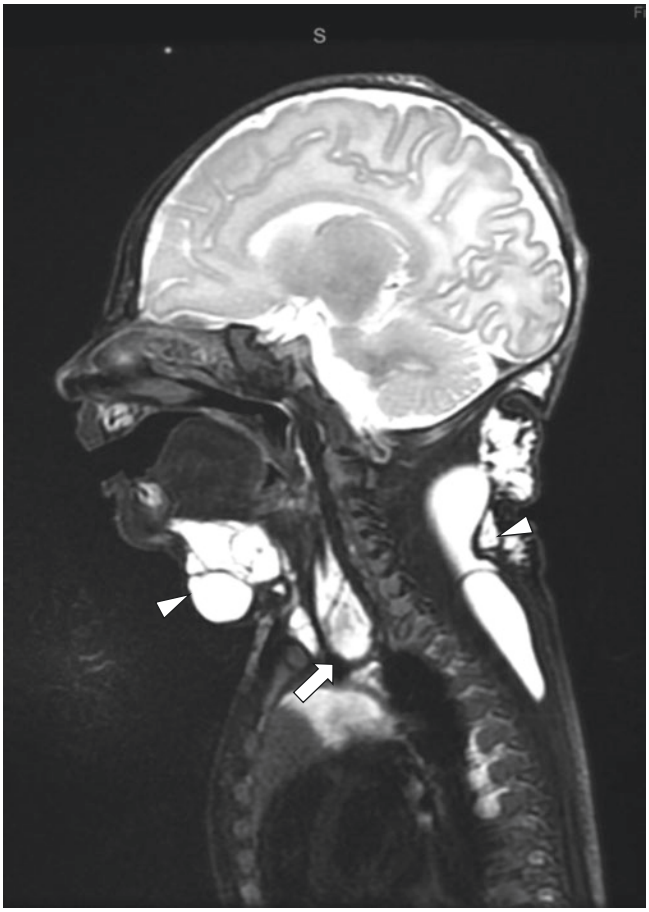

Fig. 2.37 Lymphatic malformation in a 2-day-old girl who presented with respiratory distress and palpable neck mass. Sagittal nonenhanced T2-weighted 3D CUBE (GE) MR image shows multiple hyperintense cystic lesions (*arrowheads*) in the neck, one in the anterior part of the trachea and descending in the anterior mediastinum (*arrow*)

Castleman Disease

Castleman disease is a lymphoproliferative disorder that causes lymphadenopathy in different parts of the body [122]. Castleman disease can be unicentric, when lymphadenopathy is located in a single anatomical region (i.e., mediastinum), or multicentric, when it involves multiple regions. The latter is also associated with signs of inflammatory disease, including hepatosplenomegaly, cytopenias, and organ dysfunction due to excessive pro-inflammatory hypercytokinemia. Castleman disease can be idiopathic but is associated with infection of human herpes virus 8 (HHV-8) in immunodeficient patients (i.e., HIV-positive children). Castleman disease is also associated with malignancies such as lymphoma. Castleman disease can occur at any age, although it is more common in young adults [122]. Castleman disease is usually asymptomatic, especially in the unicentric form. If symptoms occur, they are typically related to mass effect from enlarged lymph nodes, which can cause extrinsic compression on adjacent structures including large airways. Common sites of lymphadenopathy are the chest (24%), neck (20%), abdomen (18%), and retroperitoneum (14%) [122].

On CXR, Castleman disease typically presents as a mediastinal or hilar mass [123]. On CT, Castleman disease typically appears as a soft tissue mass with homogeneous contrast enhancement which may cause vessel or airway compression [123]. MR imaging typically demonstrates a solid mass which is isointense to skeletal muscle on T1-weighted images, hyperintense to skeletal muscle on T2-weighted images, and avidly enhancing on post-contrast images (Fig. 2.38) [123]. PET-CT/MR imaging is also used to detect positive lymph nodes in other anatomical regions. Although the described imaging features are suggestive of Castleman disease, biopsy is necessary to confirm the diagnosis [123].

When possible, surgical resection is the method of choice to treat lymphadenopathy from Castleman disease [122]. When an enlarged lymph node from Castleman disease is close to a major structure such as large airways or major blood vessels, radiation therapy or chemotherapy is more often used for treatment.

Neuroblastoma

Neuroblastomas are tumors arising from cells in the adrenal medulla and sympathetic nervous system [124]. Neuroblastomas have variable behavior ranging from benign tumors that show spontaneous regression to aggressive malignant tumors with metastatic disease [124]. Neuroblastoma is the third most common childhood cancer, after leukemia and brain tumors, and is the most common solid extracranial tumor in children [125, 126]. It is usually diagnosed in the first 2 years of life. Symptoms in children with neuroblastoma vary based on the number and location of tumors and can include both local and systemic symptoms. Approximately half of affected patients present with localized disease, with the remainder having distant metastases, especially to the bones and liver.

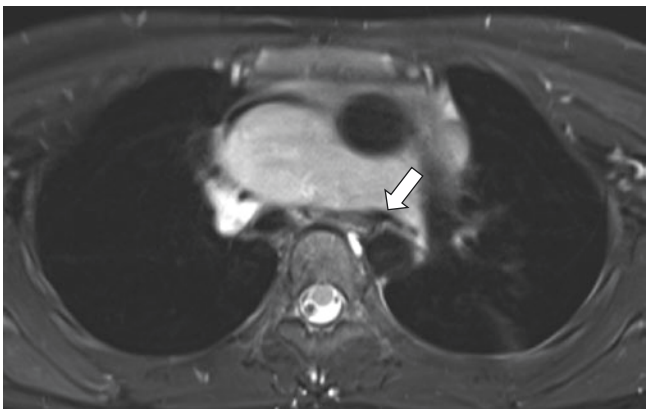

Fig. 2.38 Castleman disease in a 13-year-old girl who presented with respiratory distress. Axial nonenhanced T2-weighted HASTE MR image with fat suppression shows large hyperintense mediastinal lymph node compressing the left main bronchus (*arrow*)

The most common primary site is the adrenal gland, where neuroblastomas present as asymptomatic abdominal masses or with symptoms related to local compression (abdominal pain, distension, constipation) or hypertension due to catecholamine production [125, 126]. Neuroblastoma can extend to the spinal canal and can lead to spinal cord compression and paraplegia [126, 127]. A common location in infants is the cervical and thoracic region, where they can cause compression of the symphatic trunk leading to Horner syndrome (unilateral ptosis, anhidrosis, and miosis) or compress the airways resulting in respiratory symptoms (Fig. 2.39).

Cross-sectional imaging studies such as CT and MR imaging are used to detect neuroblastoma as well as assess local extension of the tumor, lymph node involvement, and distant metastasis [125, 126]. When located in the neck and mediastinum, neuroblastoma tends to encase vascular structures and compresses large airways. On CT, neuroblastoma appears as a heterogeneous mass with contrast enhancement

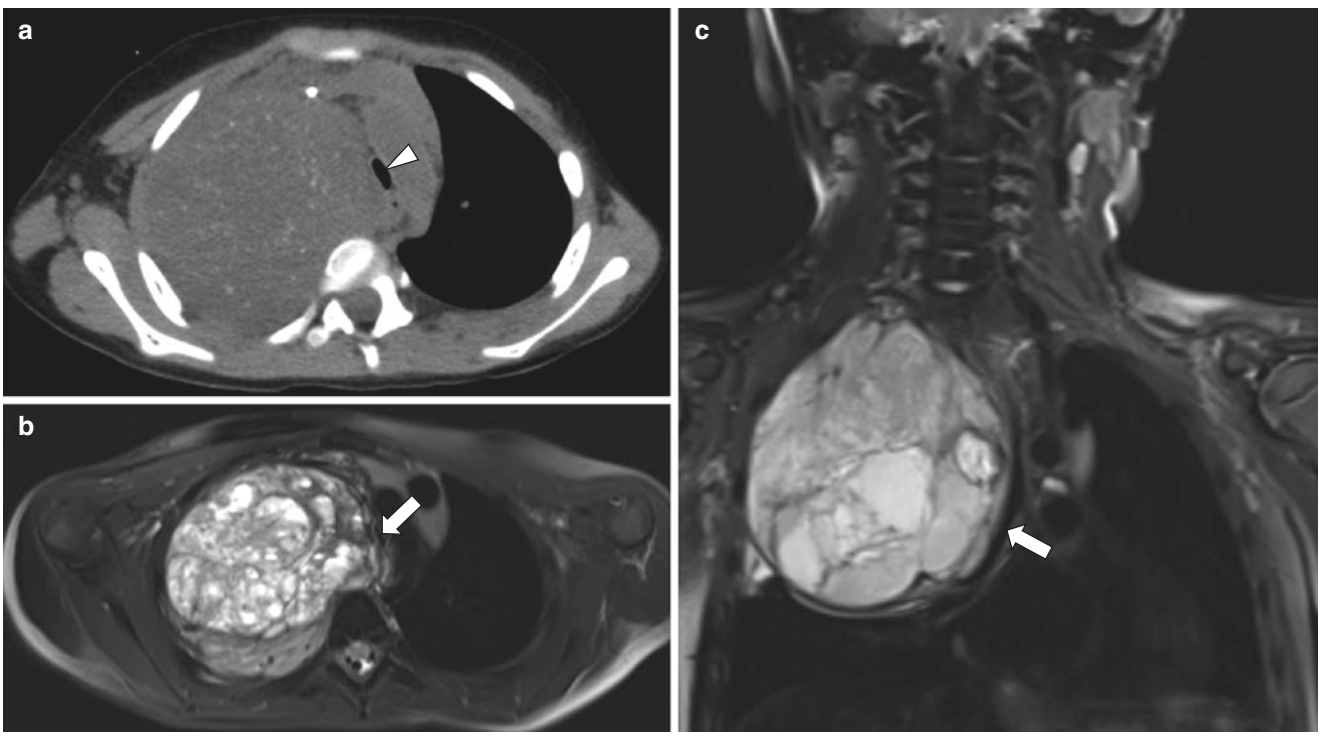

Fig. 2.39 Thoracic neuroblastoma in a 5-year-old boy who presented with respiratory distress. (**a**) Axial nonenhanced soft tissue window setting CT image shows large mass containing calcifications in the right upper thorax compressing the trachea (*arrowhead*). (**b**) Axial nonenhanced T2-weighted HASTE MR image with fat suppression shows heterogeneous hyperintense signal within the mass compressing the trachea (*arrow*). (**c**) Coronal nonenhanced T2-weighted HASTE MR image with fat suppression shows mass compressing the trachea and right main bronchus (*arrow*)

and often shows calcifications. On MR imaging, neuroblastoma appears as a heterogeneous mass that is hyperintense on T2-weighted images and restricts diffusion on diffusion-weighted images. Gadolinium contrast often improves the visualization of tumor infiltration into adjacent tissues and tumor vascularity.

The current treatment of neuroblastoma includes a combination of radiation therapy, chemotherapy, and surgical resection [125]. Prognosis depends on the location, extension, and genetics of the tumor and the age at presentation. In general, the younger the age at diagnosis, the better the survival rate.

Conclusion

The use of MR imaging for large airway evaluation in the pediatric population has three unparalleled advantages over CT. These include the absence of ionizing radiation, the ability to perform dynamic imaging, and excellent tissue characterization. Currently, various congenital and acquired pediatric large airway disorders can be evaluated using MR imaging. New sequences provide image quality comparable to CT with practical protocols that can be applied in daily clinical setting. Careful attention to patient preparation, protocol optimization, and appropriate use of sedation are the keys to obtaining diagnostic pediatric large airway MR imaging. Future developments in MR imaging and post-processing techniques (i.e., automatic MR imaging airways segmentation tools) have a great promise to further increase the use of MR imaging in pediatric patients and expand its clinical applications in various pediatric large airway disorders.

References

1. Tiddens HAWM, Kuo W, van Straten M, Ciet P. Paediatric lung imaging: the times they are a-changin. Eur Respir Rev. 2018;27(147):170097. https://doi.org/10.1183/16000617.0097-2017.
2. Ciet P, Tiddens HAWM, Wielopolski PA, et al. Magnetic resonance imaging in children: common problems and possible solutions for lung and airways imaging. Pediatr Radiol. 2015;45(13):1901–15.
3. Baez JC, Ciet P, Mulkern R, Seethamraju RT, Lee EY. Pediatric chest MR imaging: lung and airways. Magn Reson Imaging Clin N Am. 2015;23(2):337–49.
4. Lee EY, Zucker EJ, Restrepo R, Daltro P, Boiselle PM. Advanced large airway CT imaging in children: evolution from axial to 4-D assessment. Pediatr Radiol. 2013;43(3):285–97.
5. Liszewski MC, Hersman FW, Altes TA, Ohno Y, Ciet P, Warfield SK, Lee EY. Magnetic resonance imaging of pediatric lung parenchyma, airways, vasculature, ventilation, and perfusion: state of the art. Radiol Clin North Am. 2013;51(4):555–82. Review.
6. Baez JC, Seethamraju RT, Mulkern R, Ciet P, Lee EY. Pediatric chest MR imaging: sedation, techniques, and extracardiac vessels. Magn Reson Imaging Clin N Am. 2015;23(2):321–35.
7. Edwards AD, Arthurs OJ. Paediatric MRI under sedation: is it necessary? What is the evidence for the alternatives? Pediatr Radiol. 2011;41(11):1353–64.
8. Lutterbey G, Wattjes MP, Doerr D, Fischer NJ, Gieseke J, Schild HH. Atelectasis in children undergoing either propofol infusion or positive pressure ventilation anesthesia for magnetic resonance imaging. Pediatr Anesth. 2007;17(2):121–5.
9. Salamon E, Lever S, Kuo W, Ciet P, Tiddens HA. Spirometer guided chest imaging in children: it is worth the effort! Pediatr Pulmonol. 2017;52(1):48–56.
10. Gai ND, Malayeri A, Agarwal H, Evers R, Bluemke D. Evaluation of optimized breath-hold and free-breathing 3D ultrashort echo time contrast agent-free MRI of the human lung. J Magn Reson Imaging. 2016;43(5):1230–8.
11. Dournes G, Grodzki D, Macey J, Girodet PO, Fayon M, Chateil JF, et al. Quiet submillimeter MR imaging of the lung is feasible with a PETRA sequence at 1.5 T. Radiology. 2015;279(1):328.
12. Chandarana H, Block KT, Winfeld MJ, Lala SV, Mazori D, Giuffrida E, et al. Free-breathing contrast-enhanced T1-weighted gradient-echo imaging with radial k-space sampling for paediatric abdominopelvic MRI. Eur Radiol. 2014;24(2):320–6.
13. Kishida Y, Koyama H, Seki S, Yoshikawa T, Kyotani K, Okuaki T, et al. Comparison of fat suppression capability for chest MR imaging with Dixon, SPAIR and STIR techniques at 3 tesla MR system. Magn Reson Imaging. 2018;47:89–96.
14. Gibiino F, Sacolick L, Menini A, Landini L, Wiesinger F. Free-breathing, zero-TE MR lung imaging. MAGMA. 2015;28(3):207–15.
15. Kumar S, Rai R, Stemmer A, Josan S, Holloway L, Vinod S, et al. Feasibility of free breathing lung MRI for radiotherapy using non-Cartesian k-space acquisition schemes. Br J Radiol. 2017;90(1080):20170037.
16. Bates AJ, Higano NS, Hysinger EB, et al. Quantitative assessment of regional dynamic airway collapse in neonates via retrospectively respiratory-gated ^{1}H ultrashort echo time MRI. J Magn Reson Imaging. 2019;49(3):659–67.
17. Liszewski MC, Ciet P, Lee EY. MR imaging of lungs and airways in children. Magn Reson Imaging Clin N Am. 2019;27(2):201–25.
18. Ciet P, Wielopolski P, Manniesing R, Lever S, de Bruijne M, Morana G, et al. Spirometer-controlled cine magnetic resonance imaging used to diagnose tracheobronchomalacia in paediatric patients. Eur Respir J. 2014;43(1):115–24.
19. Ciet P, Boiselle PM, Heidinger B, et al. Cine MRI of tracheal dynamics in healthy volunteers and patients with tracheobronchomalacia. AJR Am J Roentgenol. 2017;209(4):757–61.
20. Berrocal T, Madrid C, Novo S, Gutiérrez J, Arjonilla A, Gómez-León N. Congenital anomalies of the tracheobronchial tree, lung, and mediastinum: embryology, radiology, and pathology. Radiographics. 2004;24:e17.
21. Holbert JM, Strollo DC. Imaging of the normal trachea. J Thorac Imaging. 1995;10(3):171–9.
22. Kotecha S. Lung growth for beginners. Paediatr Respir Rev. 2000;1(4):308–13.
23. Biyyam DR, Chapman T, Ferguson MR, Deutsch G, Dighe MK. Congenital lung abnormalities: embryologic features, prenatal diagnosis, and postnatal radiologic-pathologic correlation. Radiographics. 2010;30(6):1721–38.
24. Griscom NT, Wohl ME. Dimensions of the growing trachea related to body height. Am Rev Respir Dis. 1985;131(6):840–4.
25. Griscom NT, Wohl ME. Dimensions of the growing trachea related to age and gender. AJR Am J Roentgenol. 1986;146(2):233–7.
26. Jeffrery PK. The development of large and small airways. Am J Respir Crit Care Med. 1988;157(5 Part 2):S174–80.

27. Lawrence DA, Branson B, Oliva I, Rubinowitz A. The wonderful world of the windpipe: a review of central airway anatomy and pathology. Can Assoc Radiol J. 2015;66(1):30–43.
28. Boiselle PM. Imaging of the large airways. Clin Chest Med. 2008;29(1):181–93.
29. Boiselle PM, Lee KS, Ernst A. Multidetector CT of the central airways. J Thorac Imaging. 2005;20(3):186–95.
30. Breatnach E, Abbott GC, Fraser RG. Dimensions of the normal human trachea. AJR Am J Roentgenol. 1984;142(5):903–6.
31. Hewitt RJ, Butler CR, Maughan EF, Elliott MJ. Congenital tracheobronchial stenosis. Semin Pediatr Surg. 2016;25(3):144–9.
32. Uchida DA, Morgan-wallace V, Richards K, Seidelman J, Muntz HR. Congenital tracheal stenosis masquerading as asthma in an adolescent: the value of spirometry. Clin Pediatr (Phila). 2009;48(4):432–4.
33. Applegate KE, Goske MJ, Pierce G, Murphy D. Situs revisited: imaging of the heterotaxy syndrome. Radiographics. 2013;19(4):837–52; discussion 853–4.
34. Yoneyama H, Kondo C, Yamasaki A, Nakanishi T, Sakai S. Comparison of situs ambiguous patterns between heterotaxy syndromes with polysplenia and asplenia. Eur J Radiol. 2015;84(11):2301–6.
35. Loomba R, Shah PH, Anderson RH, Arora Y. Radiologic considerations in heterotaxy: the need for detailed anatomic evaluation. Cureus. 2016;8(1):e470. https://doi.org/10.7759/cureus.470.
36. Shapiro AJ, Zariwala MA, Ferkol T, Davis SD, Sagel SD, Dell SD, et al.; Genetic Disorders of Mucociliary Clearance Consortium. Diagnosis, monitoring, and treatment of primary ciliary dyskinesia: PCD foundation consensus recommendations based on state of the art review. Pediatr Pulmonol. 2016;51(2):115–32. Review.
37. Donnelly LF, Jones BV, Strife JL. Imaging of pediatric tongue abnormalities. AJR Am J Roentgenol. 2000;175(2):489–93.
38. Lo Casto A, Salerno S, Cannizzaro F, Caronia A, Bencivinni F, Barbiera F, et al. MRI findings in lingual venous malformations. Dentomaxillofacial Radiol. 2003;32(5):333–6.
39. Perkins JA. Overview of macroglossia and its treatment. Curr Opin Otolaryngol Head Neck Surg. 2009;17(6):460–5.
40. Fujioka M, Young LW, Giardany BR. Radiographic evaluation of adenoidal size in children: ratio. AJR Am J Roentgenol. 1979;133(3):401–4.
41. Fernbach SK, Brouillette RT, Riggs TW, Hunt CE. Radiologic evaluation of adenoids and tonsils in children with obstructive sleep apnea: plain films and fluoroscopy. Pediatr Radiol. 1983;13(5):258–65.
42. Fricke BL, Donnelly LF, Shott SR, Kalra M, Poe SA, Chini BA, Amin RS. Comparison of lingual tonsil size as depicted on MR imaging between children with obstructive sleep apnea despite previous tonsillectomy and adenoidectomy and normal controls. Pediatr Radiol. 2006;36(6):518–23.
43. Donnelly LF, Casper KA, Chen B. Correlation on cine MR imaging of size of adenoid and palatine tonsils with degree of upper airway motion in asymptomatic sedated children. AJR Am J Roentgenol. 2002;179(2):503–8.
44. John SD, Swischuk LE. Stridor and upper airway obstruction in infants and children. Radiographics. 1992;12(4):625–43.
45. Schroeder JW, Holinger LD. Congenital laryngeal stenosis. Otolaryngol Clin North Am. 2008;41(5):865–75.
46. Sanford E, Saadai P, Lee H, Slavotinek A. Congenital high airway obstruction sequence (CHAOS): a new case and a review of phenotypic features. Am J Med Genet A. 2012;158A(12):3126–36.
47. Ryan G, Somme S, Crombleholme TM. Airway compromise in the fetus and neonate: prenatal assessment and perinatal management. Semin Fetal Neonatal Med. 2016;21(4):230–9.
48. Guimaraes CV, Linam LE, Kline-Fath BM, Donnelly LF, Calvo-Garcia MA, Rubio EI, et al. Prenatal MRI findings of fetuses with congenital high airway obstruction sequence. Korean J Radiol. 2009;10(2):129–34.
49. Goyal A, Jones MO, Couriel JM, Losty PD. Oesophageal atresia and tracheo-oesophageal fistula. Arch Dis Child Fetal Neonatal Ed. 2006;91(5):381–4. Review.
50. Garge S, Rao KL, Bawa M. The role of preoperative CT scan in patients with tracheoesophageal fistula: a review. J Pediatr Surg. 2013;48(9):1966–71.
51. Hochart V, Verpillat P, Langlois C, Garabedian C, Bigot J, Debarge VH, et al. The contribution of fetal MR imaging to the assessment of oesophageal atresia. Eur Radiol. 2015;25(2):306–14.
52. Higano NS, Bates AJ, Tkach JA, Fleck RJ, Lim FY, Woods JC, Kingma PS. Pre- and post-operative visualization of neonatal esophageal atresia / tracheoesophageal fistula via magnetic resonance imaging. J Pediatr Surg Case Rep. 2018;29:5–8.
53. Kovesi T, Rubin S. Long-term complications of congenital esophageal atresia and/or tracheoesophageal fistula. Chest. 2004;126(3):915–25.
54. Yedururi S, Guillerman RP, Chung T, Braverman RM, Dishop MK, Giannoni CM, Krishnamurthy R. Multimodality imaging of tracheobronchial disorders in children. Radiographics. 2008;28(3):e29.
55. Desir A, Ghaye B. Congenital abnormalities of intrathoracic airways. Radiol Clin North Am. 2009;47(2):203–25.
56. Ghaye B, Szapiro D, Fanchamps J-M, Dondelinger RF. Congenital bronchial abnormalities revisited. Radiographics. 2001;21(1):105–19.
57. Doolittle AM, Mair EA. Tracheal bronchus: classification, endoscopic analysis, and airway management. Otolaryngol Neck Surg. 2002;126(3):240–3.
58. Newman B. Congenital bronchopulmonary foregut malformations: concepts and controversies. Pediatr Radiol. 2006;36(8):773–91.
59. Kinsella BD, Sissons G, Williams MP. The radiological imaging of bronchial atresia. Br J Radiol. 1992;65(776):681–5. Review.
60. Gipson MG, Kristopher W, Hurth KM. Bronchial atresia. Radiographics. 2009;29(5):1531–5.
61. Thacker PG, Rao AG, Hill JG, Lee EY. Congenital lung anomalies in children and adults: current concepts and imaging findings. Radiol Clin North Am. 2014;52(1):155–81.
62. Fievet L, D'Journo XB, Guys JM, Thomas PA, De Lagausie P. Bronchogenic cyst: best time for surgery? Ann Thorac Surg. 2012;94(5):1695–9.
63. Kirmani B, Kirmani B, Sogliani F. Should asymptomatic bronchogenic cysts in adults be treated conservatively or with surgery? Interact Cardiovasc Thorac Surg. 2010;11(5):649–59.
64. Hall NJ, Stanton MP. Long-term outcomes of congenital lung malformations. Semin Pediatr Surg. 2017;26(5):311–6.
65. Malhotra A, White DP. Obstructive sleep apnoea. Lancet. 2002;360(9328):237–45. Review
66. Chang SJ, Chae KY. Obstructive sleep apnea syndrome in children: epidemiology, pathophysiology, diagnosis and sequelae. Korean J Pediatr. 2010;53(10):863–71.
67. Thakkar K, Yao M. Diagnostic studies in obstructive sleep apnea. Otolaryngol Clin North Am. 2007;40(4):785–805.
68. Mello Junior CF, Guimarães Filho HA, Gomes CA, Paiva CC. Radiological findings in patients with obstructive sleep apnea. J Bras Pneumol. 2013;39(1):98–101. [Article in English, Portuguese].
69. Donnelly LF. Obstructive sleep apnea in pediatric patients: evaluation with cine MR sleep studies. Radiology. 2007;236(3):768–78.
70. Brockbank JC. Update on pathophysiology and treatment of childhood obstructive sleep apnea syndrome. Paediatr Respir Rev. 2017;24:21–3.
71. Torretta S, Rosazza C, Pace ME, Iofrida E, Marchisio P. Impact of adenotonsillectomy on pediatric quality of life: review of the literature. Ital J Pediatr. 2017;43(1):107.

72. Kaditis AG, Alonso Alvarez ML, Boudewyns A, Alexopoulos EI, Ersu R, Joosten K, et al. Obstructive sleep disordered breathing in 2- to 18-year-old children: diagnosis and management. Eur Respir J. 2016;47(1):69–94.
73. Lee EY, Litmanovich D, Boiselle PM. Multidetector CT evaluation of tracheobronchomalacia. Radiol Clin North Am. 2009;47(2):261–9. Review.
74. Carden KA, Boiselle PM, Waltz DA, Ernst A. Tracheomalacia and tracheobronchomalacia in children and adults: an in-depth review. Chest. 2005;127(3):984–1005.
75. Lee KS, Sun MR, Ernst A, Feller-Kopman D, Majid A, Boiselle PM. Comparison of dynamic expiratory CT with bronchoscopy for diagnosing airway malacia: a pilot evaluation. Chest. 2007;131(3):758–64.
76. Boiselle PM, O'Donnell CR, Bankier AA, Ernst A, Millet ME, Potemkin A, Loring SH. Tracheal collapsibility in healthy volunteers during forced expiration: assessment with multidetector CT. Radiology. 2009;252(1):255–62.
77. Fraga JC, Jennings RW, Kim PC. Pediatric tracheomalacia. Semin Pediatr Surg. 2016;25(3):156–64.
78. Snijders D, Barbato A. An update on diagnosis of tracheomalacia in children. Eur J Pediatr Surg. 2015;25(4):333–5.
79. Centers for Disease Control and Prevention. Surveillance, Epidemiology, and Outbreak Investigations Branch. Division of Tuberculosis Elimination. Epidemiology of Pediatric Tuberculosis in the United States, 1993–2016. 21 Jun 2017. https://www.cdc.gov/tb/publications/slidesets/pediatrictb/PediatricTB_SlideSet_TextOnly_2016.pdf. Accessed 29 July 2019.
80. European Centre for Disease Prevention and Control/WHO Regional Office for Europe. Tuberculosis surveillance and monitoring in Europe. Report 2018. 2016 data. 2018. Sotkcholm: European Centere for Disease Prevention and Control; 2018. https://ecdc.europa.eu/sites/portal/files/documents/ecdc-tuberculosis-surveillance-monitoring-Europe-2018-rev1.pdf. Accessed 29 July 2019.
81. Fonseca-Santos J. Tuberculosis in children. Eur J Radiol. 2005;55(2):202–8.
82. Burrill J, Williams CJ, Bain G, Conder G, Hine AL, Misra RR. Tuberculosis: a radiologic review. Radiographics. 2007;27(5):1255–73.
83. Nachiappan AC, Rahbar K, Shi X, Guy ES, Mortani Barbosa EJ Jr, Shroff GS, et al. Pulmonary tuberculosis: role of radiology in diagnosis and management. Radiographics. 2017;37(1):52–72.
84. Rizzi EB, Schinina' V, Cristofaro M, Goletti D, Palmieri F, Bevilacqua N, et al. Detection of pulmonary tuberculosis: comparing MR imaging with HRCT. BMC Infect Dis. 2011;11:243. https://doi.org/10.1186/1471-2334-11-243.
85. Sodhi KS, Sharma M, Saxena AK, Mathew JL, Singh M, Khandelwal N. MRI in thoracic tuberculosis of children. Indian J Pediatr. 2017;84(9):670–6.
86. Gaensbauer J, Broadhurst R. Recent innovations in diagnosis and treatment of pediatric tuberculosis. Curr Infect Dis Rep. 2019;21(1):4. https://doi.org/10.1007/s11908-019-0662-0.
87. Chu JH, Feudtner C, Heydon K, Walsh TJ, Zaoutis TE. Hospitalizations for endemic mycoses: a population-based national study. Clin Infect Dis. 2006;42(6):822–5.
88. Kirchner SG, Hernanz-Schulman M, Stein SM, Wright PF, Heller RM. Imaging of pediatric mediastinal histoplasmosis. Radiographics. 1991;11(3):365–81.
89. Rossi SE, McAdams HP, Rosado-de-Christenson ML, Franks TJ, Galvin JR. Fibrosing mediastinitis. Radiographics. 2001;21(3):737–57. Review.
90. Wheat LJ, Freifeld AG, Kleiman MB, Baddley JW, McKinsey DS, Loyd JE, Kauffman CA. Infectious Diseases Society of America. Clinical practice guidelines for the management of patients with histoplasmosis: 2007 update by the Infectious Diseases Society of America. Clin Infect Dis. 2007;45(7):807–25.
91. Güneyli S, Ceylan N, Bayraktaroğlu S, Acar T, Savaş R. Imaging findings of vascular lesions in the head and neck. Diagn Interv Radiol. 2014;20(5):432–7.
92. Flors L, Leiva-Salinas C, Maged IM, Norton PT, Matsumoto AH, Angle JF, et al. MR imaging of soft-tissue vascular malformations: diagnosis, classification, and therapy follow-up. Radiographics. 2011;31(5):1321–40.
93. Darrow DH. Management of infantile hemangiomas of the airway. Otolaryngol Clin North Am. 2018;51(1):133–46.
94. Fortes HR, Ranke FMV, Escuissato DL, Araujo Neto CA, Zanetti G, Hochhegger B, et al. Laryngotracheobronchial papillomatosis: chest CT findings. J Bras Pneumol. 2017;43(4):259–63. [Article in English, Portuguese].
95. Fortes HR, von Ranke FM, Escuissato DL, Araujo Neto CA, Zanetti G, et al. Recurrent respiratory papillomatosis: a state-of-the-art review. Respir Med. 2017;126:116–21.
96. Fortman BJ, Kuszyk BS, Urban BA, Fishman EK. Neurofibromatosis type 1: a diagnostic mimicker at CT. Radiographics. 2001;21(3):601–12.
97. Meredith HC, Valicenti JF. Solitary neurofibroma of the trachea. Br J Radiol. 1978;51(603):218–9.
98. Kami YN, Chikui T, Okamura K, Kubota Y, Oobu K, Yabuuchi H, et al. Imaging findings of neurogenic tumours in the head and neck region. Dentomaxillofacial Radiol. 2012;41:18–23.
99. Reviron-Rabec L, Girerd B, Seferian A, Campbell K, Brosseau S, Bergot E, et al. Pulmonary complications of type 1 neurofibromatosis. Rev Mal Respir. 2016;33(6):460–73.
100. Pappo AS, Meza JL, Donaldson SS, Wharam MD, Wiener ES, Qualman SJ, et al. Treatment of localized nonorbital, nonparameningeal head and neck rhabdomyosarcoma: lessons learned from intergroup rhabdomyosarcoma studies III and IV. J Clin Oncol. 2003;21(4):638–45.
101. Weiss AR, Lyden ER, Anderson JR, Hawkins DS, Spunt SL, Walterhouse DO, et al. Histologic and clinical characteristics can guide staging evaluations for children and adolescents with rhabdomyosarcoma: a report from the Children's Oncology Group Soft Tissue Sarcoma Committee. J Clin Oncol. 2013;31(26):3226–32.
102. Tröbs RB, Mader E, Friedrich T, Bennek J. Oral tumors and tumor-like lesions in infants and children. Pediatr Surg Int. 2003;19(9–10):639–45.
103. Friedman ER, John SD. Imaging of pediatric neck masses. Radiol Clin North Am. 2011;49(4):617–32.
104. Tranvinh E, Yeom KW, Iv M. Imaging neck masses in the neonate and young infant. Semin Ultrasound CT MRI. 2015;36(2):120–37.
105. LaPlante JK, Pierson NS, Hedlund GL. Common pediatric head and neck congenital/developmental anomalies. Radiol Clin North Am. 2015;53(1):181–96.
106. Jeung M-Y, Gasser B, Gangi A, et al. Bronchial carcinoid tumors of the thorax: spectrum of radiologic findings. Radiographics. 2002;22(2):351–65.
107. Fauroux B, Aynie V, Larroquet M, Boccon-Gibod L, Ducou le Pointe H, Tamalet A, Clément A. Carcinoid and mucoepidermoid bronchial tumours in children. Eur J Pediatr. 2005;164(12):748–52.
108. Doppman JL, Pass HI, Nieman LK, Findling JW, Dwyer AJ, Feuerstein IM, et al. Detection of ACTH-producing bronchial carcinoid tumors: MR imaging vs CT. AJR Am J Roentgenol. 1991;156(1):39–43.
109. Amini B, Huang SY, Tsai J, Benveniste MF, Robledo HH, Lee EY. Primary lung and large airway neoplasms in children: current imaging evaluation with multidetector computed tomography. Radiol Clin North Am. 2013;51(4):637–57.
110. Baxi AJ, Chintapalli K, Katkar A, Restrepo CS, Betancourt SL, Sunnapwar A. Multimodality imaging findings in carcinoid tumors: a head-to-toe spectrum. Radiographics. 2017;37(2):516–36.

111. ElNayal A, Moran CA, Fox PS, Mawlawi O, Swisher SG, Marom EM. Primary salivary gland–type lung cancer: imaging and clinical predictors of outcome. AJR Am J Roentgenol. 2013;201(1):W57–63.
112. Gaissert HA, Grillo HC, Shadmehr MB, Wright CD, Gokhale M, Wain JC, Mathisen DJ. Uncommon primary tracheal tumors. Ann Thorac Surg. 2006;82(1):268–73.
113. Butrynski JE, D'Adamo DR, Hornick JL, Dal Cin P, Antonescu CR, Jhanwar SC, et al. Crizotinib in ALK-rearranged inflammatory myofibroblastic tumor. N Engl J Med. 2010;363(18):1727–33.
114. Lee EY, Greenberg SB, Boiselle PM. Multidetector computed tomography of pediatric large airway diseases: state-of-the-art. Radiol Clin North Am. 2011;49(5):869–93.
115. Semple T, Calder A, Owens CM, Padley S. Current and future approaches to large airways imaging in adults and children. Clin Radiol. 2017;72(5):356–74.
116. Kiryu T, Hoshi H, Matsui E, Iwata H, Kokubo M, Shimokawa K, Kawaguchi S. Endotracheal/endobronchial metastases : clinicopathologic study with special reference to developmental modes. Chest. 2001;119(3):768–75.
117. Downing GJ, Kilbride HW. Evaluation of airway complications in high-risk preterm infants: application of flexible fiberoptic airway endoscopy. Pediatrics. 1995;95(4):567–72.
118. Gaebler C, Mueller M, Schramm W, Eckersberger F, Vécsei V. Tracheobronchial ruptures in children. Am J Emerg Med. 1996;14(3):279–84.
119. Kiyan G, Gocmen B, Tugtepe H, Karakoc F, Dagli E, Dagli TE. Foreign body aspiration in children: the value of diagnostic criteria. Int J Pediatr Otorhinolaryngol. 2009;73(7):963–7.
120. Hunter TB, Taljanovic MS. Foreign bodies. Radiographics. 2003;23(3):731–57. Review.
121. Bhat V, Bhat V, Salins P. Imaging spectrum of hemangioma and vascular malformations of the head and neck in children and adolescents. J Clin Imaging Sci. 2014;4:31. https://doi.org/10.4103/2156-7514.135179.
122. Talat N, Belgaumkar AP, Schulte KM. Surgery in Castleman's disease: a systematic review of 404 published cases. Ann Surg. 2012;255(4):677–84.
123. Madan R, Chen J, Trotman-Dickenson B, Jacobson F, Hunsaker A. The spectrum of Castleman's disease: mimics, radiologic pathologic correlation and role of imaging in patient management. Eur J Radiol. 2012;81(1):123–31.
124. Tomolonis JA, Agarwal S, Shohet JM. Neuroblastoma pathogenesis: deregulation of embryonic neural crest development. Cell Tissue Res. 2018;372(2):245–62.
125. Brisse HJ, McCarville MB, Granata C, Krug KB, Wootton-Gorges SL, Kanegawa K, et al.; International Neuroblastoma Risk Group Project. Guidelines for imaging and staging of neuroblastic tumors: consensus report from the International Neuroblastoma Risk Group Project. Radiology. 2011;261(1):243–57.
126. Swift CC, Eklund MJ, Kraveka JM, Alazraki AL. Updates in diagnosis, management, and treatment of neuroblastoma. Radiographics. 2018;38(2):566–80.
127. Golden CB, Feusner JH. Malignant abdominal masses in children: quick guide to evaluation and diagnosis. Pediatr Clin North Am. 2002;49(6):1369–92.